EFFECTS OF GRID DESIGN ON LEAD-ACID BATTERY PERFORMANCE

A Thesis Submitted to
The Graduate School of Engineering and Sciences of
Izmir Institute of Technology
In Partial Fulfillment of the Requirements for the Degree of

MASTER OF SCIENCE

in Energy Engineering

by
Tuğçe İŞLER

July 2017
İZMİR

We approve the thesis of **Tuğçe İŞLER**

Examining Committee Members:

Assist. Prof. Dr. Özgenç EBİL
Department of Chemical Engineering, İzmir Institute of Technology

Prof. Dr. Seher Fehime ÇAKICIOĞLU ÖZKAN
Department of Chemical Engineering, İzmir Institute of Technology

Assoc. Prof. Dr. Güler NARİN
Department of Chemical Engineering, Uşak University

28 July 2017

Assist. Prof. Dr. Özgenç EBİL
Supervisor, Department of Chemical Engineering, İzmir Institute of Technology

Assist. Prof. Dr. Ayben TOP
Co-Supervisor, Department of Chemical Engineering, İzmir Institute of Technology

Prof. Dr. Gülden GÖKÇEN AKKURT
Head of the Department of Energy Engineering

Prof. Dr. Aysun SOFUOĞLU
Dean of Graduate School of Engineering and Sciences

ACKNOWLEDGEMENTS

First of all, I am heartily thankful to my supervisor and my mentor, Assist. Prof. Dr. Özgenç EBİL. His knowledge has broadened my mind during my studies. His encouragements were motivating, and his sincerity made everything easy. His support became the reason of my willing to learn and study more in the pursuit of excellence during this Master's thesis study.

I am grateful to my dear friends Elif ŞAHİN and Esra HACIBEKTAŞOĞLU for their friendship, sincerity, patience, and encouragements. I appreciate all their selfless help in the most crucial times.

I would also like to thank my roommates Selcan ATEŞ, Merve ÖZPİRİN and Gizem CİHANOĞLU for their friendship, motivations, helping me throughout my M.Sc. thesis, and also, I will miss our coffee break.

I express my special thanks to Salih Murat KARA for his help, understanding, motivations, and limitless support.

At last, I want to express my gratitude to the most important people in my life, to my parents Gülseren and Kaya ŞAHİN, my sister Saliha Seren ŞAHİN and my grandmother Saliha ŞAHİN. Their unlimited patience with me and their supports about anything that I have decided, especially coming in Izmir to make a graduate study, made everything so easy for me to focus on my studies.

ABSTRACT

EFFECTS OF GRID DESIGN ON LEAD-ACID BATTERY PERFORMANCE

In today's world, approximately 88 percent of the total energy demand is supplied by fossil fuels; however, it has become clear that; other energy sources are needed due to limited fossil fuels. The demand for energy can most effectively be filled by renewable energy sources as installed energy storage capacity is growing rapidly. If renewable energy sources advance enough to fulfill the high demand, earth-friendly, clean and sustainable energy will help to protect the environment, thus ensuring a healthier life for future generations.

Energy storage systems are essential in this endeavor, and in order to become more prevalent, storage systems for renewable energy sources must supply electricity without interruption as much as possible. As an electrochemical storage, a battery with a high level of performance, high energy density and life cycle could offer a viable solution for electricity storage provided that battery cost should be economically viable.

This thesis aims to improve the geometry of the grid used in lead acid batteries in order to obtain a more uniform current and potential distribution, and minimize the potential drop for improved battery performance. A 3D mathematical model was developed using finite element method to evaluate the behavior of the grid under various conditions. Five different porous grid geometries were simulated under different loads and optimum grid geometry was identified. The 3D mathematical model of the lead-acid battery based on finite element method was simulated under certain conditions in order to evaluate the effect of grid geometry on battery performance.

ÖZET

IZGARA TASARIMININ KURŞUN-ASİT BATARYA ÜZERİNDEKİ ETKİLERİ

Günümüzde enerji ihtiyacının yaklaşık %88i fosil yakıtlardan elde edilmektedir fakat bu yakıtların sınırlı olmasından dolayı başka enerji kaynaklarına da ihtiyaç duyulmaktadır. Enerji talebi, kurulu enerji depolama kapasiteleri hızla büyüdüğünden yenilenebilir enerji kaynaklarıyla giderilebilir. Yenilenebilir enerji kaynakları, yüksek talebi karşılayacak kadar ilerlerse, çevre dostu, temiz ve sürdürülebilir enerji çevrenin korunmasına yardımcı olacak, böylece gelecek kuşaklar için daha sağlıklı bir yaşam sağlayacaktır.

Enerji depolama sistemleri bu çabada önemlidir ve yenilenebilir enerji kaynakları için depolama sistemlerinin daha yaygın hale gelmesi için mümkün olduğunca kesintisiz elektrik sağlamalıdır. Elektrokimyasal depolama olarak, yüksek performans, yüksek enerji yoğunluğu ve uzun ömrü olan bir pil, pil maliyetinin ekonomik açıdan uygun olması koşuluyla elektrik depolama için uygun bir çözüm sunabilir.

Bu tezin amacı daha düzgün bir akım ve potansiyel dağılımı elde etmek ve potansiyel düşüşü en aza indirgeyerek daha gelişmiş bir batarya performansı elde etmek için kurşun asit bataryalarda kullanılan ızgaranın geometrisini geliştirmektir. Çeşitli koşullar altında ızgaranın davranışını değerlendirmek için sonlu elemanlar yöntemi kullanılarak bir 3D matematiksel model geliştirildi. Farklı yükler altında beş farklı gözenekli ızgara geometrisi simüle edildi ve optimum ızgara geometrisi tespit edildi. Sonlu elemanlar yöntemine dayanan üç boyutlu matematiksel kurşun asit batarya modeli, ızgara geometrisinin pil performansı üzerindeki etkisini değerlendirmek için belirli koşullar altında simüle edildi.

TABLE OF CONTENTS

LIST OF FIGURES

LIST OF TABLES

Table **Page**

CHAPTER 1

INTRODUCTION

Energy storage problems are increasing worldwide, despite the fact that renewable energy sources are being used more effectively. However, this problem can be solved with new and efficient energy storage technologies. One such technology is the battery. This thesis aims to improve lead-acid battery performance by grid design optimization using models based on finite element analysis method.

1.1. Energy and Environment

Energy, in the simplest way, means the ability to do work. All organisms require the energy to live. Energy is used everywhere connected to human activities and surrounds us as the center of our lives. The main energy source is the Sun. Energy is taken from the Sun by the Earth and joins the life cycle. Energy supports both our bodies and our whole society, so it is crucial to life. Yet, in the modern day, energy consumption has increased day-by-day, so the energy crisis is starting to be a critical problem. There is also a need to switch from fossil fuels to renewable energy sources such as solar, wind, geothermal. Other energy sources that are non-renewable energy such as fossil fuels (oil, natural gas, coal), including nuclear energy, can be harmful to nature, as they bring about environmental pollution. Besides, in the end, they are limited. In contrast, renewable energy is almost infinite as well as being clean, cheap, and environmentally friendly.

In addition, as we realize these critical conditions, non-renewable energy sources have been exploited, excessively. But, now we use both the renewable and the non-renewable energy. Figure 1.1 indicates a simple energy source flowchart to demonstrate what kinds of energy sources exist. The renewable and the non-renewable energy sources are primary energy sources. The secondary energy sources are derived from the primary energy sources such as electricity, gasoline, alcohol fuels (gasohol).

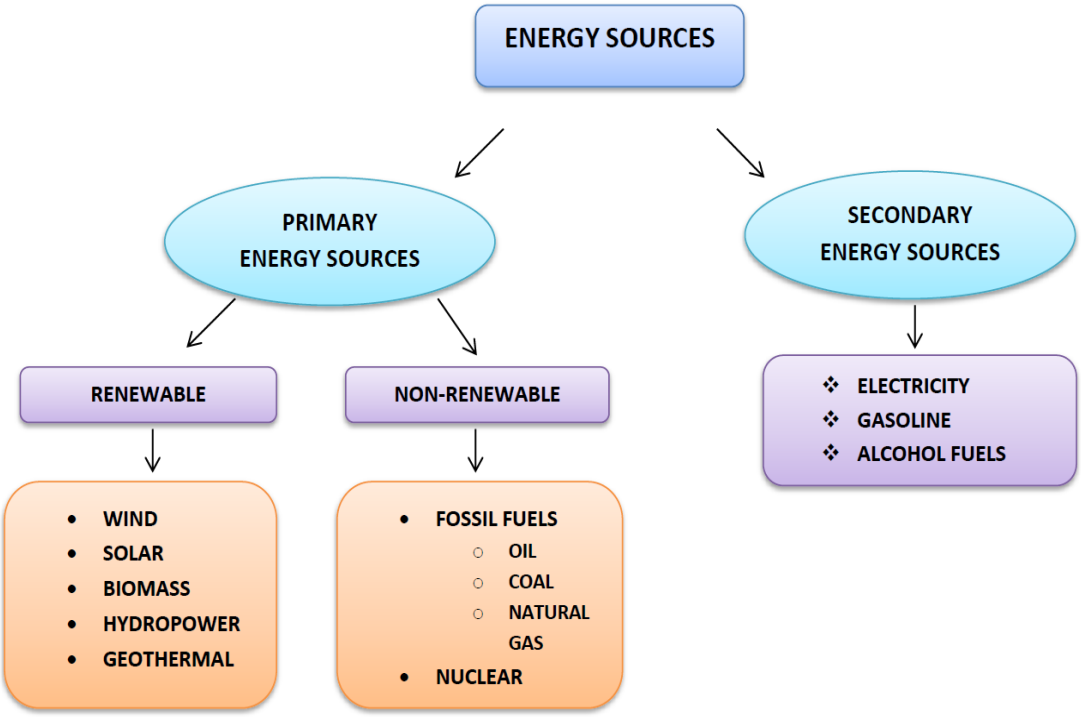

Figure 1.1. Energy sources flowchart.

As it is shown, energy can be used in many forms like electrical energy, mechanical energy, and chemical energy, that is, it can be transformed from one form to another via various applications. Figure 1.2 indicates the global energy consumption between 1965-2013. The usage of renewable energy is very little bit compared to the usage of the non-renewable energy sources (Tverberg, 2015). Although there is still an abundance of fossil fuels, the non-renewable energy sources are limited. On the contrary, the renewable energy sources are needed to maintain the energy supply, so their usage should be increased.

Traditional energy sources, mainly fossil fuels like oil, coal, and natural gas, are also a greatly powerful factors for the economy and many industries. As the name implies, fossil fuels come from fossils. The creation of fossil fuel takes a long period; they come from the organic remains of prehistoric plants and animals. While the fossil fuels are carried easily to the power stations, the transportation of renewable energy is harder. The other comparison to consider between renewable and non-renewable energy is the installation of power stations whereas non-renewable energy stations can be built almost anywhere, solar and wind farm cannot. However, fossil fuels bring about detrimental effects regarding environment and human health due to emission of CO_2. Furthermore, fossil fuels give rise to global warming. However, renewable energy

sources represent a real alternative to fossil fuels as they do not generate significant emission, prevent acid rain, and slow down global climate change.

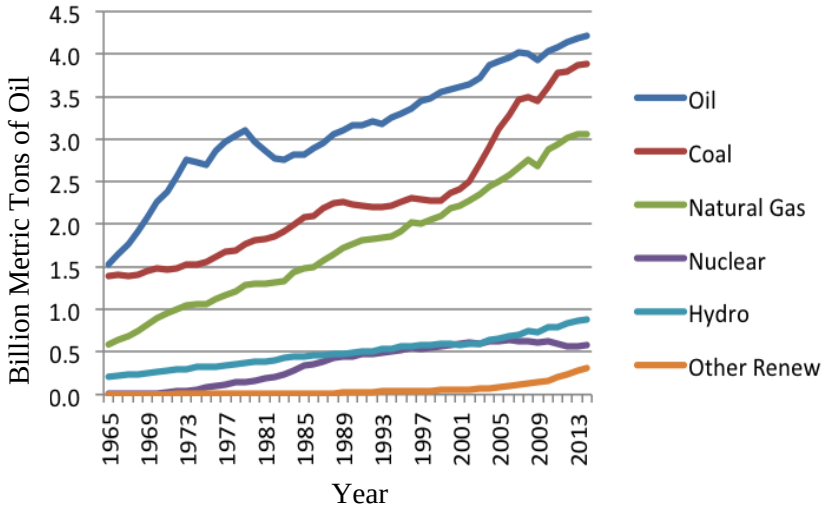

Figure 1.2. World Energy Consumption for Each Fuel (Source: Tverberg, 2015).

Although the potential of renewable energy sources is immense, they cannot be utilized effectively due to the energy storage problem. Even though a great deal energy sources exist in nature, energy storage problem is an obstacle to use them effectively. Until the energy storage problem is solved, our energy demand cannot be met on a large scale. There are three main energy storage technologies: mechanical, chemical and thermal storage. Among these technologies, electrochemical storage technology is significant, electricity generated from solar and wind farms will mostly rely only on electrochemical energy storage in the near future. Electrochemical storage converts the chemical energy to the electrical energy. In order to provide uninterrupted energy for longer durations at different load ranges require batteries with high energy and power densities and long operational lifetimes. The loads might vary from 3 mAh for watches and memory backup to 2000 Ah for submarine and standby power supplies (Linden & Reddy, 2001).

Electric energy is one of the most the important type of energy since almost all human activities involve using electrical energy. Electrical energy is clean and can be transmitted to where needed. However, electrical energy generated from renewable sources is intermittent and cannot provide sufficient energy at all times. The bottleneck for renewable energy technology development is the electrical energy storage. Electrical

energy must be stored in another form (mechanical, thermal or chemical) and be ready for instant use (Ter-Gazarian, 2011).

1.2. Batteries

A battery is a kind of energy storage device that converts chemical energy into electrical energy via electrochemical reactions, which are oxidation and reduction (redox reactions). A battery is composed of cells connected in series or parallel. A cell is the basic electrochemical unit. The main components of a cell are two electrodes; positive and negative, and an electrolyte. In a positive electrode that is a cathode, a reduction process occurs. During the process, a positive electrode gains electrons while the negative electrode (an anode) is oxidized, therefore losing electrons. If the chemical reactions are reversible, these batteries are called chargeable or secondary batteries. In this case, the cycle is reversed by charging the battery so that the reduction happens in the anode and the oxidation takes place in the cathode. Now, the cathode is the negative electrode while the anode is the positive electrode. The electrolyte provides electrical conductivity through ions and may be liquid or gel. Anode and cathode electrodes are usually submerged or embedded in the electrolyte.

When examining Table 1.1, the lead-acid battery appears to have the worst battery performance contrasting with the others in specific energy and the energy density. Even though there are many high-performance batteries, LA battery has kept hold of its leadership for 150 years because there is still not a viable alternative battery (in terms of cost) for most applications. Moreover, lead-acid batteries are utilized in the automotive sector and the renewable energy applications, as it has such a large application area.

When looking at the history of batteries, their invention reaches until as early as 200 years ago. The first battery was made in 1800 by Alessandro Volta who is a physics professor at University of Pavia in Italy (M. Barak, 2006). Following this in 1836, Copper-zinc battery was built by Daniell Cell, with the invention of Daniell battery; the restrictions of Voltaic cell were solved. Next is the lead-acid battery, the first rechargeable battery, by Gaston Planté, who solved the non-reversible battery problem. These inventions continued with Carbon zinc wet cell invention by Lechanche in 1866 and a Carbon zinc dry cell that is the first dry cell battery by Gassner in 1888. Later, the various types of nickel cadmium batteries were developed by Junger and Neumann in

1899 and 1946, respectively. One of the most important battery inventions is the lithium-ion battery which found a wide variety of applications. However, lithium is expensive, limited and Li batteries suffer from safety issues. Today, the future of the battery technology seems to be moving towards metal-air battery technologies (R. Vasant Kumar, Sarakonsri, 2010).

Table 1.1. Characteristics of batteries (Source: Kiehne, 2000).

	Lead-Acid, Pb-PbO	**Nickel-Metal Hydride, Ni-MH**	**Sodium-Nickel Chloride Na-$NiCl_2$**	**Sodium-Sulfur, Na-S**	**Li-Ion**
Operating temperature (°C)	<45	<45	235-350	285-330	<50
Electrolyte	H_2SO_4	KOH	β" –ceramic	β" –ceramic	LiPF6
Cell OCV (V)	2.0	1.2	2.58	2.1	4.0
Specific energy (Wh/kg)	25-35	40-60	100-120	110	80-120
Energy density (Wh/L)	50-90	120-160	160-200	135	200
Specific power (W/kg)	150	Up to 1000	150-180	<75	500-800

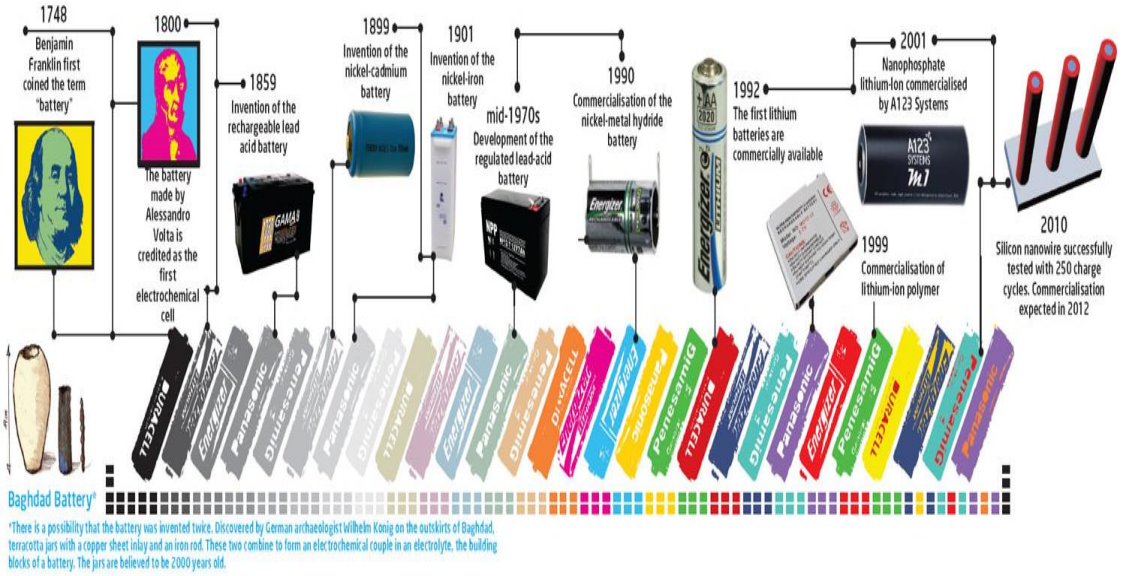

Figure 1.3. History of the battery (Source: Caris, 2014).

CHAPTER 2

LEAD ACID BATTERY

In this chapter, the invention of lead acid (LA) battery, how has it been developed, and also its fabrication will be discussed. In addition, since the LA battery grid is an important factor in this thesis, it has been addressed in detail. Furthermore, its area of usage in industry and its type will be explained. Finally, thermodynamics and the kinetics of batteries will be described.

2.1. History of LA Battery

Gaston Planté, a French physicist, invented the first storage battery or the accumulator. The history of LA started with Gaston Planté's experiment in 1860. In the light of the invention of lead-acid battery, lead-acid battery applications have spread in the various applications of energy storage, especially the starter batteries (Besenhard, 1999).

2.1.1. Brief Introduction

Electricity is one of the biggest discoveries of humanity. The technology has developed rapidly due to the discovery of electricity. In order to generate electricity as an energy source, the methods of electrochemical storage began advancing at the beginning of the nineteenth century (Pavlov, 2011). Battery technology started with Alessandro Volta's experiments. However, considering all batteries technologies, the lead acid battery has the greatest significance because it has the largest usage capacity. It is cheap, safe, and handy. However, lead acid batteries are heavy, have low specific energy density, and can lead to contamination. Despite these disadvantages, lead acid battery became the most popular on the market. Its story started with supplying emergency power before being popular in the automotive industry. The first one was the stand-by battery, and it was used for vital energy requirements, such medical

applications and emergency lights. Later, the lead acid battery applications have spread in various areas (R M Dell, D A J Rand, 2001).

2.1.2. Development of LA Battery

The lead-acid battery history can be separated in the three parts. The first period started with Planté's invention and covers a time frame between 1860 and 1910. In that period, simple electrode structures (plates) and practical manufacturing techniques were mostly used. The pasted plate was produced by Faure at the end of the century in 1881, while the tubular plate was introduced at the beginning of the century. Moreover, the "double sulphate theory" was published by Gladstone and Tribe in 1880. The theory was discussed for years and it was reintroduced many years later as the overall discharge-charge (Technical Marketing Staff of Gates Energy Products, 1998):

$$PbO_2 + Pb + 2H_2SO_4 \leftrightarrow 2PbSO_4 + 2H_2O \quad (2.1)$$

The basic electrochemical redox reaction was used in its final forms by 1910, and also it was known that the negative and positive electrodes sponge lead and lead-oxide respectively transform to the lead sulfate in dilute sulfuric acid solution. The second period convers 1910 to 1950 time frame and continued with the plate technology and cell manufacturing with some advances. The cycle life increased significantly due to the introduction of lignin expanders into the negative plates. Another improvement was the usage of antimony-free grid alloys in 1935. As a result of the scientific discoveries, the double sulphate theory was confirmed, and the thermodynamics data of the negative and positive electrodes immersed in sulfuric acid were determined. The third period has continued since 1950. One of the technological progresses was a change of hard rubber; instead of it, polypropylene began to be used for battery casings. Better batteries were developed by optimizing grid design with thinner plates and improving active mass material, so it had the high discharge. As well as those developments, the experiments of lead and lead dioxide electrodes were conducted to understand and enhance its performance. Galvanostat, constant current generators, and potentiostat, an individual electrode potential regulating method, and sweep generators were launched for use. Thus, these progressions caused the new innovation in mass transport area. Considering all the developments, the kinetics of electrode process

attracted attention instead of thermodynamics. There was a debate about the lead-acid battery as an outdated technology in 1960, but was also shown that other battery technologies could not provide a better alternative than the lead-acid battery. In addition, the new car technologies, like electrical cars, have encouraged lead-acid battery research, as well as generating plenty of lead (Ruetschi, 1977).

Electrical cars began to be produced at the end of the 19th century before electrical submarines in World War I. LA batteries found use in those applications. In fact, batteries started to be employed firstly in lighting systems as an emergency power supplier in railway coaches, railway-signaling systems, radio receiving-transmitting systems, and in ships. Finally, when the lead acid battery continued to be developed alongside the internal combustion engine, it was used for car lighting systems, and for engine starting too. Hence, all electrical necessity of modern vehicles utilized LA batteries. Traction batteries applications have grown in forklifts, electric motorcycles, terrain vehicles, and other electric vehicles, as well. Even though the new battery technologies that have more performance, cycle life, and other advantages have been developed for a long time, no battery could take the place of the lead-acid battery (R M Dell, D A J Rand, 2001). The automotive battery with starting-lighting-ignition is the leading type of battery. This battery is also used for wind and the solar power applications (Jürgen Garche & Dayer, 2009). The first practical version of the lead-acid battery technology, the first rechargeable battery, was invented by Gaston Planté in 1859. The technology has proceeded about 165 years with many applications in the automotive and telecommunication industry. Before Planté, in 1801, Johann Ritter discovered the first accumulator known as RITTERsche Saule. It has copper plates and NaCI- impregnated sheets of paper that separates the electrodes from each other. He also started his experiment with lead, tin and zinc plates in 1802, and therefore designed the first accumulator system. However, he did not use sulfuric acid electrolyte, therefore lead-acid battery was invented after 50 years. In addition, Kastner, Nobili, Schonbein, and Wheatstone conducted tests with lead and lead dioxide immersed in sulfuric acid solution between 1810-1843.

Wilhelm Joseph Sinsteden studied a few electrochemical cells to compare their currents. While using the lead electrodes and diluted sulfuric acid for electrolyte in the test cell, he developed the working principles of the lead-acid battery, and the electrical storage capability of this system. He published an article related to his findings in 1854. Planté was different from the other scientists in electrochemistry arena, because of his

other interests in paleontology, and theology. He discovered the working principle of lead acid battery, too, but his discovery was unconnected to Sinsteden's study in 1859. However, he noticed that the importance of the lead acid battery, and unlike Sinsteden, he made technical cells, and accumulators. After those discoveries, while in the United States, Charles Kirchoff improved a solution accumulator using platinum electrodes in a $Pb(NO_3))_2/Pb(CH_3COO)_2$ electrolyte. In Germany, Wilhelm Siemens found a new lead acid battery system with carbon electrodes saturated with lead salt in an acid solution in 1860. Progress of the lead acid battery technology continued for years. In 1881, Faure used a porous active mass on the lead electrodes to cover the grid. This is the second major step for development of lead acid battery technology after Planté's invention. The mass of lead plates was preserved because of lead oxide. The same year, Volckmar devised grids and pasted electrodes and Scudamore Sellon fabricated a lead antimony grid plate**.** Also, Brush, an American scientist, exploited Faure's idea in his accumulator (J. Garche, 1990; Pavlov, 2011). The use of rectangular vents in lead plates, the weight of plates was made lighter. Thereby, the modern pasted plate battery arose. Especially for the automotive industry, this type of battery is the most commonly used one at the present time. After these developments, small developments on lead-acid battery technology continued for usability in the field. For instance, low maintenance or maintenance free types were developed to avoid adding distilled water over time (R M Dell, D A J Rand, 2001)**.** However, the pasted electrodes were not used in extensive application areas until the middle of 20^{th} century. That invention caused the development of new separators, and in consequence of the new separators, the service life of the electrodes was enhanced. Next, Volckmar's plates were improved by Tudor in 1886. Before that, Philippart manufactured another type of electrodes by packing it as a round lead with active mass, and the active mass was covered by ebonite rings in 1883. In the same year, Woodward made iron-clad electrodes by using rubber pipes (J. Garche, 1990)**.** Before the development of new separators, there were still problems about the lower cycle life of pasted plate battery. During the deep discharge, providing electricity to an electric vehicle, the cycle life and capacity were being reduced significantly. This problem helped the invention of new technologies such as fibre glass retainer and tubular plate battery (R M Dell, D A J Rand, 2001)**.**

When it comes to the grid developments, Fabraky and Schenek applied a circular segment to grid pattern and improved cell performance. When Aron added cellulose to active material in 1882, it was observed that the electrolyte diffuses into the active mass

in depth. Müller in 1882 and Gardner in 1886 obtained patents related to carbon addition to the active mass to increase conductivity. In 1885, to reduce the mass of the active mass holder, the Primary Battery Company Limited devised the combination grid compounded collector and embedded in the insulator grid made up of hard rubber. Later, Gestel submitted a grid consisting of copper clothed with lead in 1888; which is now manufactured by Hagen Batterie AG. Gelled battery, one of the last lead acid battery technology, was developed by Zierfuss in 1888 and Schoop in 1890 to generate a leak-proof accumulator. The electrolyte included SiO_2 and H_2SO_4. This invention was important to prevent leakage from the accumulator. Today, the gel electrolyte is still used in a sealed battery (J. Garche, 1990).

In the twentieth century, major developments occurred regarding new materials and new technologies, for instance, polypropylene, polyethylene copolymer or acrylonitrile butadiene styrene replaced the ebonite battery case. While lead alloy with 11% antimony known as 'hard lead' was used for sometime, the new lead alloys were developed to produce a lighter lead alloy called low-antimony lead alloys, adding Sn, Ag, and As. Grid technology continued performance improvement with new methods such as die-cut technology at the end of the 20^{th} century (Pavlov, 2011).

The oldest lead acid battery technology has diluted sulfuric acid electrolyte that is called flooded cell design. Due to the liquid electrolyte, this type of battery has some disadvantages; some of them are the necessity of a vent for the cell to leave off the gasses during charging, and position of the cell. The cell must always be the upright position because sulfuric acid might leas; hence, it can be dangerous for environment and people. This situation gave rise to a sheltered battery to prevent these problems. Sealed batteries emerged to overcome issues related to liquid electrolyte. For example, Valve-regulated lead-acid (VRLA) batteries were invented to prevent leakage problem (R M Dell, D A J Rand, 2001). VRLA battery was a great novelty because the electrolyte did not need any water during operational lifetime (Jürgen Garche & Dayer, 2009). In VRLA batteries, while reducing oxygen at the negative electrode, recombination process for hydrogen does not take place due to slowness of oxidation of the gas at the positive electrode. Therefore, for every cell, a valve must be assembled in order to save extreme pressure, due to incomplete of oxygen recombination. A VRLA battery can be placed in every position without problem of leakage. It is also easy to use for consumers and engineers. Yet, despite these developments, the lead acid battery still

has some problems about the performance and the cycle life (R M Dell, D A J Rand, 2001).

When we look at the present, various type of lead acid batteries are used widely. The lead-acid battery has been particularly employed in electric scooters, electric bicycles, and electric vehicles since early 2000s. It is also used as starter battery in automotive industry. The lead-acid battery market reached $ 60.3 billion in 2010. It is expected to reach $ 103.8 billion in 2020.

In conclusion, the development of lead acid battery has continued since its discovery. It always preserved its position as indispensable in the battery industry because of its advantages, although lithium-ion battery technology has increased fast in last 20 years (Jung, Zhang, & Zhang, 2015). LA battery technology began with Planté and continued with valuable contributions of Faure, Sellon, Volckmar, Brush, Gladstone, Tribs, Tudor, Lucas, Phillipart, Woodward, Smith, Haring, Thomas, Bode, Voss, Ruetschi, Chan, McClelland, Jung and Kelly between 1859-2009. Despite its age and limitations, it seems LA battery technology will still be used widely in the future.

2.2. Manufacturing of LA Battery

A similar manufacturing process is used to make the lead acid battery for SLI (starting, lighting, and ignition) batteries, traction batteries, and stationary batteries. The manufacturing process can be divided into eight main steps as follows:

1) Grid Casting: Pure lead is mixed with metals and lead-alloy is prepared to improve performance. Positive and negative grids as well as small components such as the terminal and connectors are cast from liquid alloy using specific molds.

2) Lead Oxide Production: Usually pure lead ingots are exposed to surface oxidation and are grinded into powder at the same time. As an alternative process, melting, pulverization, and oxidation in air atmosphere of lead ingots can be performed sequentially. Lead oxide is oxidized up to 60% to 90% with a sufficient grain size distribution.

3) Paste Preparation: Pasting is the process by which the paste is actually integrated with the grid to produce a battery plate. The preparation is made by adding water and H_2SO_4 solution under continuous stirring while the lead oxide is fed into a mixing machine. In this stage, basic lead sulfates are produced. Hence, the prepared

paste is ready to produce the positive plates. Further, production of negative plates uses a similar process, yet the expanders are just attached to the mixture.

4) Grid Pasting: In this process, the grids are prepared as a pasted grid by employing pasting machines. Later, these pasted plated are dried in a tunnel oven and adjusted in the pallet.

5) Plate Curing: The aim of this process is to form a bond between the paste and grid. At 100% humidity and 30°C to 95°C for 24 to 72 h, pallets with plates are kept in sealed chambers. With this stage, the lead, the basic lead sulfates, the grids, and the paste are subject to some alterations which are oxidation, recrystallization, corrosion, and changing in phase composition, respectively.

6) Plate Formation: The dried plates are sent to big tanks passing an electric current through and including H_2SO_4 solution. However, the drying process is performed in an oxygen-free atmosphere. The next step is washing with water and drying the plates.

7) Production of containers, covers, vents, etc.: Plastic components are fabricated in proper molds.

8) Battery assembly: All components are assembled with the plates. Next, the container is filled with electrolyte, charged and tested for air-tightness. After, the vents are closed to remove an entry by air. Finally, the battery is ready for packing (Jung et al., 2015)**.**

For grid fabrication process, four methods are widely used:

- Gravity Casting
- Continuous Casting
- The Expanded Metal Sheet Method
- The Punched Sheet Method

While comparing these four techniques, the most popular method is still gravity casting to produce grids for lead-acid batteries. Yet, in order to make high-quality production for automobile lead-acid batteries, expanded grids and continuous cast grids are usually employed (Jung et al., 2015).

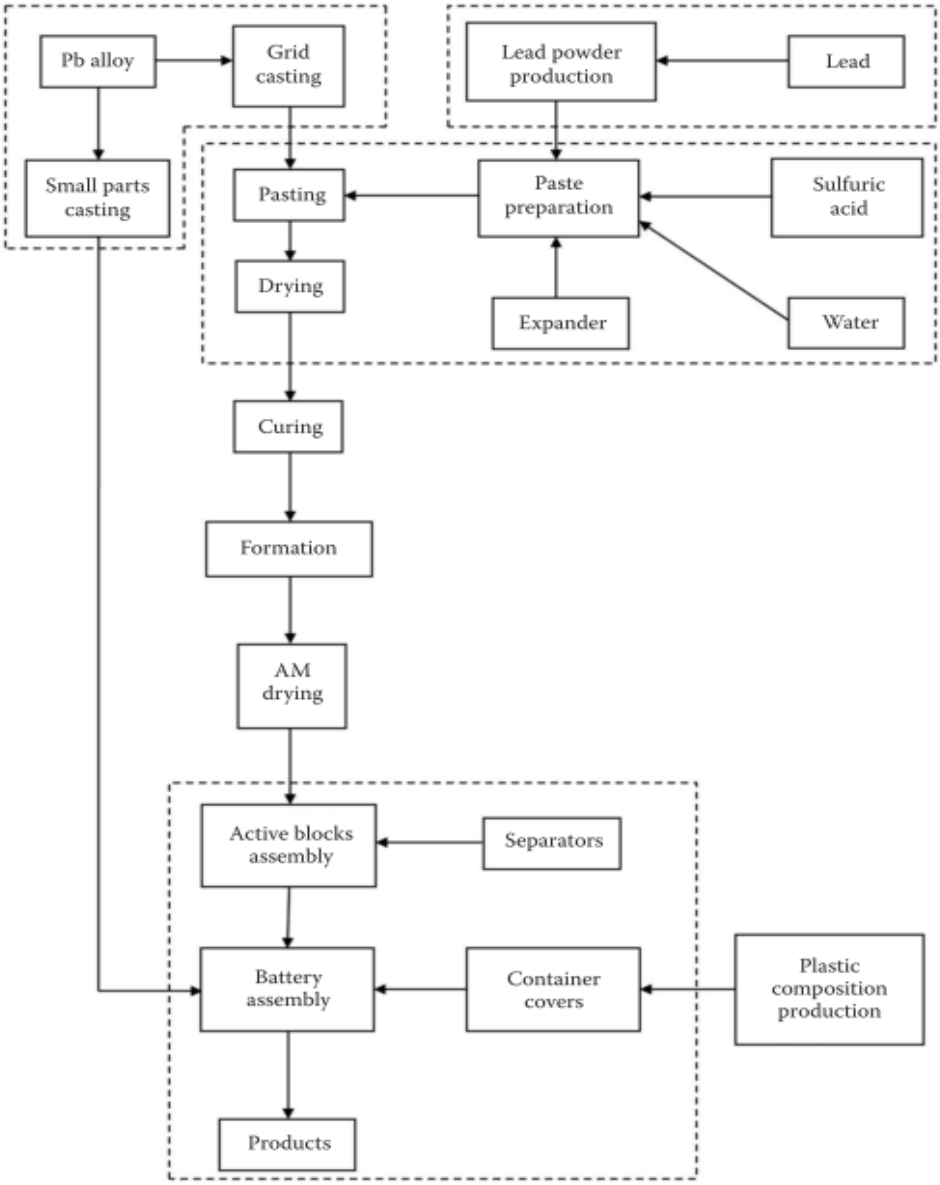

Figure 2.1. Battery manufacturing process (Source: Jung et al., 2015).

2.2.1. LA Battery Grid

Battery grid is usually made with lead alloy, due to pure led being too soft. Lead alloy usually contains lead, calcium, and tin (El-rahman, Salih, & El-Wahab, 2013). The grid serves as a conductive pathway in a battery cell; it transmits the electron. Thus, the current starts to pass from the positive electrode to the negative one. The lug is usually positioned at the top of grid in order to transport current (Vaaler, Brooman, & Fuggiti, 1982). Grid plates provide mechanical support and hold active material. It also transmits the current to everywhere in grid plate. While current transmission occurs, chemical

reactions take place, like the corrosion. For this reason, grids should not be made very thin. The operation of the positive plates at high potentials, the fast formation of a passive layer of high ohmic resistance (owing to an electrolyte that is highly corrosive), and the low potential of water decomposition limits the type of the alloy and the thickness (or thinnes) of the grid plates and lines. The manufacturers must design the physicochemical properties of lead alloys to produce battery grid plates. These are explained below.

1) Mechanical Properties: During the discharge and charge process, the plate thickness increases and decreases and then the plate grid can have dendritic growth. But, the shape of the grid must be protected, so the material must be firm and robust. On the side, the positive grid is exposed to corrosion, and there is a corrosion layer (CL). This layer can damage the grid and spoils the electrical contact.

2) Casting Properties: The alloys must be manufactured well while casting so that the grids can be loaded at a low temperature.

3) Good Weldability: While preparing the battery grid plates, the grid alloys must possess good welding properties.

4) Corrosion Resistance: During operation, positive plates continue oxidizing. Although the corrosion layer diminishes the grid corrosion rate, the process cannot be stopped completely. Furthermore, the positive plates play a significant role in the lead acid battery design in terms of the battery durability and performance.

5) High Electrical Conductivity of the CL Formed on Positive Grids: First of all, during formation of PbO_2, the corrosion of the lead grid occurs. The second step has very high specific resistance ($\sim 10^{12}$ Ω cm). Moreover, the oxidation of the formed lead oxide yields a non-stoichiometric oxide, PbO_n ($1<n<2$). Therefore, the CL oxide is oxidized to the formation of PbO_2 (10^5 to 1.2×10^{-6} Ω cm), when the value of n arrives to 1.5, and R is equal to 5×10^2 Ω cm). If the lead alloys are added to the grid, the oxidation rate of the oxides are effected in the CL. Alloying additives should be chosen, accordingly.

6) Electrical Properties: In order to decrease ohmic energy loss, high electrical conductivity is needed for lead alloys.

7) Environmental and Health Aspects: So as to protect health of the workers and environment, alloys and grids must be prepared by clean technology.

8) Economic Considerations: For low-cost grid production, cheaper alloys must be used and economically feasible fabrication method should be chosen (Pavlov, 2011).

2.3. Applications of LA Battery

The lead acid battery is one of the oldest battery technologies. Since its invention, it has been used in many applications, especially in automotive industry. Moreover, the technology continues to diverse into many new areas. Although new battery technologies were invented, no battery technologies can replace the lead-acid battery entirely because it is low cost, reliable, and easy to use. When considering automotive industry, the lead acid battery is used in more than 600 million vehicles in addition to; telecommunications, data storage, and UPS systems. In general, lead acid battery applications classify two main groups -the stationary and the automobile applications. Stationary batteries can vary from 250 Wh to 5 MWh; its applications are emergency power, local energy storage, and communication base stations. Automobile applications known as SLI are between 100 and 600 Wh (Jung et al., 2015).

2.3.1. Types of LA Battery

Valve-regulated lead-acid (VRLA), absorbed glass mat (AGM), gel, starting-lighting-ignition (SLI), and deep cycle batteries are the most commonly used varieties of LA batteries today. They are explained in the following sections:

1) Valve-Regulated Lead Acid (VRLA) Batteries: They are also known as sealed lead-acid (SLA) batteries. They are leakage, spillage and maintenance free and have a longer lifespan. In order to hinder gas leakage, there is a lid at the top of the battery. These batteries feature a pressure safety valve which lead to longer battery life and deep cycle discharge. Usually, they are made for the automobile sector (Along with the, recombinant battery). VRLA batteries are categorized into two types which are absorbed glass mat batteries and gel batteries.

2) Absorbed Glass Mat (AGM) Batteries: There is an electrolyte in the separator that is a baron silicate fiberglass mat. In this way, the electrolyte stays in the

fiberglass mat. Also, it is resistant to impacts due to mechanical strength. These batteries are known as “starved electrolyte” or “dry batteries,” as well.

3) Gel Batteries: This type of the batteries have gel electrolyte which provides more power and longer lifetime with no spillage or leakage issues associated with liquid electrolytes.

4) Starting, Lighting, and Ignition (SLI) Batteries: SLI batteries are generally made for vehicles. Depth of discharge (DOD) is important to SLI batteries, since if DOD falls under 50%, the battery can get harm, and battery life can shrink. Additionally, this battery is charged completely before starting.

5) Deep-Cycle Batteries: Deep cycle batteries can be drained to a much lower SOC value before the charging process reused in applications such as marine applications, electrical vehicles, golf carts, and forklifts. The plates are constructed thicker and more robust compared to other types LA batteries (Jung et al., 2015)**.**

2.3.2. LA Battery in Automotive Industry

Lead acid battery plays a major role in automotive sector with almost 70% of the secondary battery market in the world despite other new battery technologies with better performance (Jung et al., 2015)**.** An automotive battery is an SLI (starting, lighting, and ignition) battery. In order to supply electricity an automobile engine to start it, at least 12 volts of a SLI battery (usually six cells and connected in series) are used. Therefore, SLI battery accounted for $ 38.2 billion of the estimated annual world market in 2010. The market is anticipated to increase, especially in highly developed countries. In addition, with the improvement of electric and hybrid vehicles, this battery technology may found new markets. Figure 2.2 indicates the projection of SLI batteries until 2020. In Figure 2.2, NA, APAC, and ROW represent North America, Asia-Pacific, and Rest of World, respectively. Also, EMEA refers to Europe, the Middle East, and Africa.

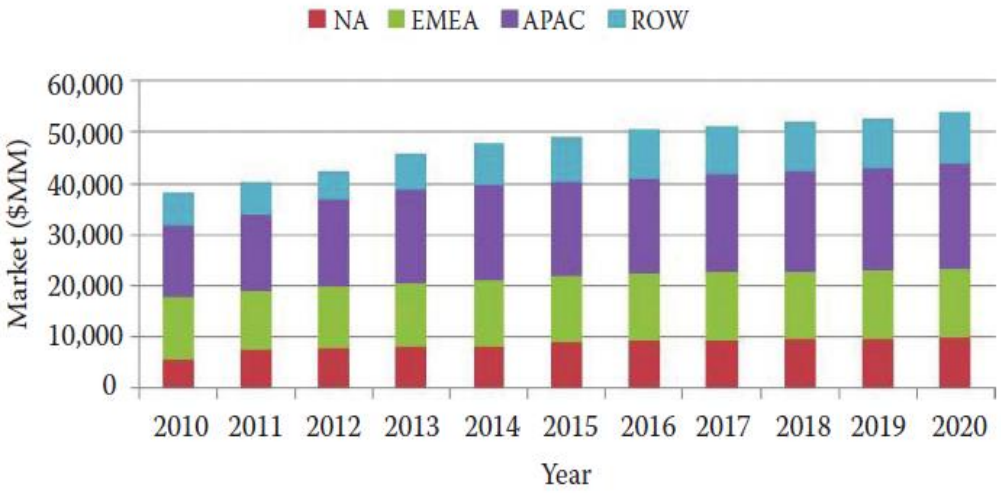

Figure 2.2. SLI battery market projection (Source: Jung et al., 2015).

Typical SLI battery applications require high-power output, low cost, rapid charge and discharge capabilities, safety, long service life and minimal maintenance. Typical applications are car starter batteries, marine vessels, light traction, hybrid electric vehicle (HEVs), electric vehicles (EVs), plug-in electric vehicles (PHEVs).

Cold cranking amps (CCAs) and reserve capacity (RC) are two important factors to determine the performance of this battery type. If a SLI battery has 12 V, CCAs refer to the number of amps a lead-acid battery at 0°F can transmit during 30 seconds by resuming at least 7.2 V. On the other hand, the RC means the amount of time (in minutes), in this time, 25 A can be carried at 80°F by keeping terminal voltage at least 10.5 V.

2.3.2.1. Hybrid Electric Vehicles

As petrol consumption was rising at the end of the twentieth century and a petrol crisis exploded, research and development efforts on the hybrid electric vehicles (HEV) increased significantly. HEVs have electrical engines supporting internal combustion engines. The types of HEV are as follows:

1) Full HEVs: If the internal combustion engine have low efficiency and high power is required, the electric battery system is generally used. However, a single electric motor can only move an automobile a short range. While running the electric

motor, the battery is discharged. It is recharged by (the internal combustion engine) and regenerative braking. It is expected the reduction of fuel consumption at the rate of 40% when the potential of the electric system exceeds 200 V.

2) Mild HEVs: In this system, the fuel consumption can be reduced between 10% and 15% based on driving mode. The electric system of the mild HEVs changes from 100 V to 200 V.

3) Micro HEVs: The fuel consumption is reduced roughly 8% in urban driving mode. The start-stop system is also employed. The system turns off the engine if the car stops.

4) Plug-in HEVs: The battery is charged in Plug-in HEVs by using the mains power supply. The battery system has a conventional automobile powered by an internal combustion engine as well as an electrical engine because the combustion engine operates as a backup power source when the battery is consumed (Pavlov, 2011).

2.4. Chemical Reactions of LA Battery

A lead acid battery cell is made of three components that are positive (cathode) and negative (anode) electrode, and the electrolyte. The negative, the positive electrode and the electrolyte are composed of porous lead, lead dioxide, and diluted sulfuric acid, respectively. The electrodes are immersed in the electrolyte. The electrolyte has a specific gravity of 1.28. Oxidation and reduction reactions occur at anode and cathode, respectively. Current passes from a cathode plate to an anode plate due to inequality of electrons between these two plates (potential difference between electrodes); chemical energy is converted to electrical energy by discharging. Therefore, the electromotive force (EMF) of the electrochemical power source is generated due to the potential difference between two electrodes. The electrolyte acts as a charge transfer medium. During the discharge process that is a spontaneous redox reaction, lead and lead dioxide are converted into lead sulfate by ions in sulfuric acid solution, and then the specific gravity of sulfuric acid solution is reduced, so it gets close to the specific gravity of water (Jung et al., 2015)**.** During discharge of the battery, lead dioxide is converted into lead sulfate and water is formed. This is the reduction reaction. At the same time, negative sulfate ions go to the lead plate, and the lead electrode gives two electrons in order to create the lead sulfate in the oxidation reaction. This is the galvanic or voltaic

cell. For an electrolyte cell, the process must be reversible or rechargeable. A load is connected externally between two electrode plates during discharge. A DC power source is used for the charging process.

These redox reactions are the half-reactions. However, in order to determine the generated current, the overall reaction must be taken into account. At the end of the overall reaction, 2 V is obtained from a cell. By connecting six cells in series, 12 V battery is made. The general reactions are given below (Kurzweil, 2010):

positive electrode : $PbO_2 + 3H^+ + HSO_4^- + 2e^- \rightarrow PbSO_4 + 2H_2O$ (2.2)

negative electrode : $Pb + HSO_4^- \rightarrow PbSO_4 + H^+ + 2e^-$ (2.3)

overall reaction : $PbO_2 + Pb + 2H_2SO_4 \leftrightarrow 2PbSO_4 + 2H_2O$ (2.4)

2.4.1. Thermodynamics and Kinetics

2.4.1.1. Potential of LA Battery

Electrochemical reactions occur at two electrodes mentioned in detail in Section 2.4. The potential at open circuit represents electromotive force of 2 V for a lead-acid battery; this is the potential difference of two electrodes. When a load is connected to an open circuit, the current starts to flow through the electrodes; it is termed as a closed circuit. Hence, the chemical energy converts to electrical energy. This is the result of changes of the material valences. The electrical energy shown as Q (J) is calculated from Formula (2.5);

$$Q = nF(E_1 - E_2) \tag{2.5}$$

where F is the Faraday constant found as 96500 Coulomb per mol, the numbers of electrons are denoted as n, E_1 and E_2 are potentials or energies of the electrodes. The electromotive force is calculated from Equation (2.6).

$$\Delta E_e = E_{PbO_2/PbSO_4} - E_{Pb/PbSO_4} \tag{2.6}$$

Equation (2.6) is the potential difference between two electrodes.

$$\Delta E_e = \Delta E_e^0 + \frac{2RT}{nF} \log \frac{a_{H_2SO_4}}{a_{H_2O}} \tag{2.7}$$

The electromotive force is affected by the concentration of H_2SO_4 and the temperature of the cell. ΔE_e^0 is calculated with Gibbs free energy of the reactants and products in the reaction stands for the EMF of the cell with no ion transfer. Its value is 2.040 V. Besides, the open cell voltage of lead acid battery changes between 2.10 and 2.13 V, and the nominal voltage is 2 V (Jung et al., 2015).

Electricity conductivity changes, depending on the electrode materials and electrolyte. As a result of Gaston Planté's experiment using Pb and PbO_2 used as electrodes immersed H_2SO_4 solution, it was observed that PbO_2 has high electron conductivity. On the side, owing to more negative equilibrium potential of $Pb/PbSO_4$ and more positive equilibrium potential of $PbO_2/PbSO_4$, composed potential difference brings out one of the most electromotive forces with sulfuric acid solution. In addition, the electrical potential is affected by the concentration of electrolyte and temperature (Pavlov, 2011). While changing specific gravity of H_2SO_4, the lead-acid battery potential at open circuit alters indirectly proportional by varying specific gravity of H_2SO_4 among 1.2 and 1.28. When the specific gravity of H_2SO_4 is 1.28 in a charged state, the open circuit voltage is 2.12 V (Jung et al., 2015)**.** The other one is the temperature effect. Then, the cell potential is measured by the Gibbs-Helmholtz Equation (2.8) shown below:

$$\Delta E_e = \frac{4.183\Delta H}{nF} + \left(\frac{d\Delta E}{dt}\right)_p \tag{2.8}$$

where ΔH is the enthalpy change in the reaction and subscript p denotes constant pressure.

In general, because of the temperature, the current density, the cell age, and the state of charge, the potential of lead acid battery fluctuates. The closed-circuit voltage happens when an electric current passes from one electrode to another one, subject to the magnitude and direction of the current and the temperature. Firstly, while discharging, the cell potential falls down from 2 V at the open circuit to 1.97 V at the

closed circuit, in other words on load. In the next step, the potential rises and comes 2 V, this continues until a certain time, and later, it decreases to 1.7 V. The sharp reduction of voltage is termed as “knee of the curve”. Initial voltage, cut-off voltage, mean working voltage, period of discharge, and initial voltage drop are all important parameters to be taken into account. Discharge voltage and charge voltage are shown as U_d and U_{ch}, respectively. The charge voltage must be higher than the open circuit voltage to reverse the process (Jung et al., 2015).

$$U_d = \Delta E_{e-} r_d I_d \tag{2.9}$$

$$U_d = \Delta E_e + r_d I_d \tag{2.10}$$

Discharge process parameters are explained below;

Initial Voltage (U_{in}): This potential is at 90% state of charge.

Cut-off Voltage (U_{cf}): The cut-off voltage is approximately 1.70 V at a 5-h discharge rate. This value is determined by the manufacturers. The cut-off voltage is affected by the discharge rate and the temperature.

Mean Working Voltage ($\bar{V}$): While taking average of N voltages value with equal time interval, mean working voltage is obtained.

$$\bar{U}_d = \frac{1}{N} \sum_1^N U_N \tag{2.11}$$

The energy and power characteristics of the battery are calculated by Equation (2.11).

Period of discharge (t_d): This time interval determined by turning on the current to the cut-off voltage is to determine the capacity of the battery.

Initial Voltage Drop (U_r): The permissible voltage drops to 1.70 V during the discharge at the electrolyte specific gravity value of 1.14. It is determined by the internal resistance of the cell. Also, initial voltage drop can induce the failure of the battery (Calvo-baza & Armenta-Deu, 1998).

Besides this, in order to determine charge efficiency, Equation (2.12) is used shown as below, also termed as charge acceptance;

$$\mathrm{ChA} = \frac{\mathrm{I} - \mathrm{I_g}}{\mathrm{I}} * 100 \tag{2.12}$$

where I and I_g are the total current and the current of water decomposition, respectively. The charge acceptance is related to the events in the charging process because during charge, $PbSO_4$ is converted into Pb and PbO_2. The charge process has three periods;

1. **Efficient charge stage:** In the course of converting of $PbSO_4$ into Pb and PbO_2, the state of charge acceptance reduces from 100% to 70% and 80%. If the cell potential charged with 0.1 A/Ah of current comes to 2.35 V, this stage ends and gas evolution occurs.

2. **Mixed Stage:** At the end of the stage, the battery is fully charged. In this process, decomposition of water progresses with the charging reaction, charge acceptance is decreased and the cell voltage rises from 2.35 to 2.50 V.

3. **Gas evolution stage:** In this stage, the cells are charged and water decomposition occurs. In addition, the self-discharge happens in the battery.

These charge stages are related to three different depths of discharge, which are 50%, 75%, and 100%. During the 75% state of charge, gas evolution voltage takes place from 2.35 to 2.40 V with a current of 0.1 A/Ah. Therefore, the efficient charge stage is over. Later, the mixed stage at a given current density is obtained as empirical while charging the battery completely.

The voltage efficiency (U_E) is determined from ratio of charge and discharge potential Equation (2.13) shown below.

$$\mathrm{U_E} = \frac{\bar{\mathrm{U}}_\mathrm{d}}{\bar{\mathrm{U}}_\mathrm{ch}} \tag{2.13}$$

This term is affected by the value of the current density. The mean voltage is 1.95 V and 2.35 V, for a 5-h discharge period and charge period, respectively, then U_E is equal to 0.83.

From Nernst equation, the potentials of the electrodes can be obtained by:

$$\mathrm{E_{Pb/PbSO4}} = \mathrm{E^0_{Pb/PbSO_4}} + (\frac{\mathrm{RT}}{\mathrm{nF}}) \ln \mathrm{k} \tag{2.14}$$

and

$$k = \frac{a_{PbSO_4}}{a_{Pb}} . a_{SO_4^{2-}} \tag{2.15}$$

where k is the equilibrium constant for the electrochemical reaction. The activities of the solid phases which are shown as a_{PbSO_4}, a_{Pb} are 1, and also when the temperature in K is taken as 298 K, R is the universal gas constant is 8.314 Joules per Kelvin per mole, F is the Faraday constant. After rearranging, we obtain;

$$E = E^0 - \frac{0.0257\ V}{n} \ln k \tag{2.16}$$

While converting the natural logarithm, the equation is multiplied with ln 10 and the equation can be written as;

$$E = E^0 - \frac{0.0592\ V}{n} \log k \tag{2.17}$$

Some parameters of the lead acid battery like the concentration of H_2SO_4, temperature, and the material, affect the battery performance. The concentration of H_2SO_4 and the temperature of the cell have an impact on the cell EMF. When the impurities are added in H_2SO_4, the decomposition of water increases, hence it can affect the battery performance badly. The effects of the concentration of sulfuric acid solution on battery performance can be collected under the four basic factors. They are the following:

1. **Open-circuit voltage (O.C.V.):** This is the voltage without current transmission, and is usually around 2 V. The potential is concerned with the concentration of the electrolyte; in order to charge battery completely, the charged voltage must be higher than open-circuit voltage at least 30-40 mV. Otherwise, battery cannot be charger fully. It also affects the charge acceptance of the cell. Therefore, the capacity and the cycle life may be lower.

2. **Electrical resistivity:** If the relative density of H_2SO_4 concentration is between 1.10 and 1.30, the battery has high power output, since the electrical conductivity of the electrolyte is higher.

3. **PbO_2 passivation:** When relative density of electrolyte reaches 1.28, the positive plate capacity and the battery cycle life are reduced due to diminishing activity of PbO_2.

4. **$PbSO_4$ solubility:** When relative denstiy of electrolyte is greater than 1.28, charge acceptance of the battery drops due to low $PbSO_4$. The cycle life shrinks due to the plate sulfation.

Three active materials of the lead acid battery lead (Pb), lead dioxide (PbO_2), and the electrolyte (H_2SO_4) play a major role in the battery performance (Nguyen, White, & Gu, 1990). The multi-valent ions and oxidants at low H_2SO_4 concentrations exert a bad influence on battery performance.

Further, the battery characteristics might have different influence on the performance for different types of lead acid batteries. In automotive industry, for SLI batteries, the important factors are cold cranking amps (CCAs) and reserve capacity (RC). For deep-cycle batteries used for generally marine vessels and electric bicycles, the cost, weight, and cycle life are considered for the battery performance, and dynamic charge acceptance and the cycle life are affected in terms of the battery performance in micro-hybrid batteries. The other battery types are industrial batteries that are motive lead acid batteries (MLA), stationary batteries, emerging grid applications, distributed renewable batteries. For MLA batteries, the crucial battery performance factor is the lifetime of the battery. The lifetime is between 500-600 cycles. The key parameter of stationary batteries as well as the emerging grid applications is a lifetime. The cost is also a requirement for the performance of emerging grid applications. The key parameters for a battery used in distributed renewable energy storage are lifetime at deep discharge and the cost. In general, cycle life is affected by the positive electrode and, the cold-temperature performance is affected by the negative electrode (Jung et al., 2015).

2.4.1.2. Effect of Temperature

Temperature is one of the most important factors for battery operation. It has direct impact on EMF. The relation between the change of energy and temperature is determined by Equation (2.8).

Lead acid batteries are also used in aircrafts. When we look at the aircraft battery, the optimum temperature is room temperature nearly 23-25℃. While it is working at high and low temperatures battery performance is reduced significantly. The minimum operation temperature is determined according to the freezing point of the electrolyte that is -70^{o} C at a specific gravity of 1.300 g cm^{-3}. When the temperature surpasses 60-70℃, battery capacity starts to decline because grid corrosion and strong gas evolution (Jürgen Garche & Dayer, 2009).

2.4.1.3. Sulfation Effects

When a lead-acid battery discharges, the active materials of lead and lead oxide are converted into lead sulfate. In the opposite case, while charging, lead sulfate ($PbSO_4$) transforms by recrystallizing. This process is called as sulfation. In order to convert lead and lead oxide form, lead sulfate creates small crystals during charge process. Yet, if the lead sulfate crystals become larger, the active materials cannot be converted. However, their original forms are transformed easily. When the negative electrode plate is considered, the growth of the nonconductive lead sulfate may give rise to the formation of the passive lead sulfate film.

In a conclusion, the battery capacity shortens with time because of sulfation of the negative plates as well as other issues explained previously. While loading the battery, there are two recharge processes that are ‘soft sulfation’ and ‘hard sulfation’. If lead-acid battery has hard sulfation due to the temperature, long periods without a full charge and lack of regular maintenance, the damage is usually irreversible. However, this problem can be avoided by keeping the battery at 100% SOC when unused. Also, pulse charging and carbon additives in negative paste can help to reduce the hard sulfation. Additionally, negative plates sulfation can depend on the concentration of the sulfuric acid solution (Jung et al., 2015). As the relative density of concentration of H_2SO_4 is higher than 1.28, $PbSO_4$ has low solubility therefore, when the charge acceptance decreases, the battery cannot be charged completely.

CHAPTER 3

LA BATTERY GRID MODELING

A grid is an important component in a lead acid cell since it serves as a current collector and a current carrier. The design and thickness of the grid affect the battery performance. However, grid thickness should be optimized with respect to cost, weight, and electrical performance. In this chapter, the different grid geometries are used in simulation of grid performance under specific conditions.

3.1. Cell Potential and Free Energy

The entropy has a tendency to increase in the universe since the formation of the universe; hence, this generates a disorder. This phenomenon is related to the second law of thermodynamics. A chemical reaction is determined to be spontaneous or non-spontaneous based on Gibbs free energy, In this case, if a change of free energy is negative, the process occurs spontaneously (Hibbert, 1993).

The electrode potential is associated with the change of the free energy. Therefore, the electromotive force is calculated by using the change in Gibbs free energy;

$$\Delta G = -NFE \tag{3.1}$$

where n is the number of electrons, F is Faraday constant, E is an electromotive force. When the EMF is positive, it shows that the reaction becomes naturally.

3.2. Faradaic and Non-Faradaic Current

The current occurs due to an inequality of the electrons. In a battery, while the chemical reactions take place with electron transfer, the electrode-electrolyte interface has the faradaic current that is complied with Faraday's law. All reactions have the faradaic current during the charge transfer; thus, they are known as electron/charge

transfer reactions and the electrodes are termed as charge transfer electrodes. On the other hand, some reactions happen at electrode-electrolyte interface without the chemical reactions such as adsorption and desorption. Those are termed non-faradaic processes. These processes do not contain electrons flow at the electrode-electrolyte interface.

3.3. Transport Number

Transport number or transference number, is a measure of the current carried by ions transport. When the ions have a positive and negative charge known as cation and anion, respectively, the transport number is called as cation and anion transport number.

3.4. Porous Electrode

The use of porous electrode arose from reducing energy loss due to activation and concentration polarizations at the electrode surface. Therefore, electrode efficiency is improved thanks to porous electrode's enhanced surface area. The porous electrode theory evolved between 1960 and 1970 (Ferg, Loyson, & Rust, 2005).

Porous electrode has a very large interfacial area per unit volume; much larger than a planar electrode. Porous electrode reactions cover the charge transfer reactions that take place at the interface of the electrolyte and electrode phases in the porous electrode, because the electrochemical reactions occur between the electrolyte and electrode interface as the heterogeneous reactions. The porous electrode establishes the charge balance of both the electrode and the pore of the electrolyte. On the other hand, the mass balance is set up for the species in the electrolyte.

The porous electrode consists of voids filled with the electrolyte and porous matrices of solids. However, in this porous media, the mass transfer related to the electrochemical reactions at the interface is too complex and not fully understood. The distribution of current in the porous electrode is based on the conductivity of the solid matrix and the electrolyte, electrochemical kinetic parameters, and physical construction of the electrode (Linden & Reddy, 2001).

3.5. The Movement of Ions

The ion movement happens in electrolyte solution in a battery. Ion interaction inside of the solution has influence on battery characteristics. Concentration gradient and electric field induce diffusion and migration of ions. The speed of ion motion is affected by its size and charge. Diffusion is seen at every species, but migration is just related to charged ions movement under an electric field. For diffusion, the Fick's first law is used:

$$\mathrm{J_i} = -\mathrm{D_i}\frac{\partial \mathrm{c_i}}{\partial \mathrm{x}} \tag{3.2}$$

where $\mathrm{J_i}$, D_i, and $\frac{\partial \mathrm{c_i}}{\partial \mathrm{x}}$ are the flux of species i, diffusion coefficient, and the concentration gradient, respectively (Brett & Brett, 1993).

3.6. Fundamental Equations

Nernst equation will be discussed in this section. Also, charge conservation in electrolyte will be described with the equations and assumptions used in this study.

3.6.1. Nernst Equation

Some reactions that occur in a battery are important to understand the behavior of the battery under non-standard conditions. A few fundamental equations are needed to explain these behaviors. One of them is the Nernst equation shown below in Equation (3.3) and (3.4) (Cynthia G. Zoski, 2007).

$$\mathrm{E} = \mathrm{E^{0\prime}} + \frac{\mathrm{RT}}{\mathrm{nF}}\ln\frac{C_0^*}{C_R^*} \tag{3.3}$$

$$\mathrm{E} = \mathrm{E^{0\prime}} + \frac{\mathrm{RT}}{\mathrm{nF}}\ln\frac{\mathrm{a_0}}{\mathrm{a_R}} \tag{3.4}$$

The Nernst equation is derived from the Gibbs free energy, and it gives cell potential under certain conditions by using the concentration (activities) of the species in the electrolyte.

3.6.2. Charge Conservation in Electrolyte

The charge density is related to the electric potential by the Poisson equation:

$$\nabla^2 V + \frac{F}{\varepsilon_0 \varepsilon_s} \sum_i z_i c_i = 0 \tag{3.5}$$

The mass and charge transport are calculated with Nernst-Planck equation mentioned in Section 3.7.1, an equation governing modes of mass transfer. When electroneutrality approximation is applied; there is no significant charge separation with respect to the approximation in bulk due to the large of the electrical force through the charged species. The assumption is given Equation (3.6) (Dickinson, Limon-Petersen, & Compton, 2011).

$$\sum_i z_i c_i = 0 \tag{3.6}$$

The charge and mass transfer occur in the ion-conducting phase. In the electrolyte, in order to understand how current density is affected, the following equation is used. Equation (3.7) provides current density balance in the electrolyte:

$$\nabla . i_l = Q_l \tag{3.7}$$

where Q_l is the current electrolyte source (A/m^3), it cannot be zero for porous electrode, the current density i_l (A/m^2) in the electrolyte is determined from Equation (3.8).

$$i_l = F \sum_{i=1}^{n} z_i \left(-D_i \nabla c_i - z_i u_{m,i} F c_i \nabla \phi_l\right) \tag{3.8}$$

The other equation describing current density in the electrolyte is a modified equation of Ohm's law that determines the charge transfer in the electrolyte:

$$i_l = -\sigma_l \nabla \phi_l + \left(\frac{\sigma_l RT}{F}\right)(1 - 2t_+)\nabla \ln c_l \tag{3.9}$$

where t_+ is the transport number.

There are the electrolyte and the solid material in the porous domain. Following expression uses the fraction of electrolyte to calculate current density for liquid in a porous media.

$$i_l = \varepsilon^{ex}(-\sigma_l \nabla \phi_l) + \varepsilon^{ex}\left(\frac{\sigma_l RT}{F}\right)(1 - 2t_+)\nabla \ln c_l \tag{3.10}$$

An applied current density can be calculated as shown in Equation (3.11):

$$i_l . n = i_{n,l} \tag{3.11}$$

where n is vector normal (perpendicular) to the boundary.

The electrode current source ($Q_s, A/m^3$) is equal to Equation (3.12) contributing the current density:

$$\nabla . i_s = Q_s \tag{3.12}$$

where i_s is shown in Equation (3.13):

$$i_s = \sigma_s \nabla \phi_s \tag{3.13}$$

and σ_s specifies the conductivity of electrode (S/m), ϕ_s is the electrode potential (V).

Equation (3.14) given below is used for the current density of solid material in the porous electrode.

$$i_s = -\varepsilon^{exm}\sigma_s \nabla \phi_s \tag{3.14}$$

In addition, the material balance equation in the electrolyte is determined by Equation (3.15).

$$\frac{\partial}{\partial t} c_l = \nabla . (D \nabla c_l) - u . \nabla c_l \tag{3.15}$$

The material balance in the porous electrodes is given as:

$$\varepsilon \frac{\partial}{\partial t} c_l = \nabla . (\varepsilon^{ex} D \nabla c_l) - u . \nabla c_l + R_l \tag{3.16}$$

where R_l is a source term (mol/s/m^3) in consequence of the electrochemical reactions. This term is related to the following expression:

$$R_l = -\sum_m \frac{a_{\upsilon,m} i_m}{n_m F} \left(\left(1 - c_l \overline{V}_e\right) \left((1 - t_+) v_{H^+,m} + t_+ v_{HSO_4^-,m} \right) - c_l \overline{V}_0 v_{H_2O,m} \right) \tag{3.17}$$

where n_m is the number of electrons involved in reaction (dimensionless), $\overline{V}_{0 v_{H_2O,m}}$ is the partial molar volume of the solvent H_2O (m^3/mol), $\overline{V}_e$ is the partial molar volume of the electrolyte (m^3/mol), $v_{H^+,m}$, $v_{HSO_4^-,m}$, $v_{H_2O,m}$ are the stoichiometric coefficients for the proton, the bisulfate ion, water in reaction m, respectively. When the electrode reactions happen in the solid material, the porosity changes due to volume changes seen below in Equation (3.18).

$$\frac{\partial \varepsilon}{\partial t} = \sum_m \frac{a_{\upsilon,m} i_m}{n_m F} \left(v_{Pb,m} \overline{V}_{Pb} + v_{PbO2,m} \overline{V}_{PbO2} + v_{PbSO4,m} \overline{V}_{PbSO4} \right) \tag{3.18}$$

The average superficial velocity in each electrode must be known since the main reactions of Pb and PbO_2 are important to the currents in each electrode.

$$u_{PbO2} = -\frac{i_l}{2F} \left(\left(\overline{V}_{PbSO4} - \overline{V}_{PbO2} - (3 - 2t_+) \overline{V}_e + 2\overline{V}_0 \right) \right) \tag{3.19}$$

$$u_{Pb} = -\frac{i_l}{2F}\left(\left(\overline{V}_{Pb} - \overline{V}_{PbSO4} - (1 - 2t_+)\overline{V}_e\right)\right) \quad (3.20)$$

Active specific surface area, $a_ʊ$ (m^2/m^3), is a significant parameter that express the area of the electrode-electrolyte interface, which is catalytically active for the porous electrode reaction. The active surface area can be determined as a function of porosity of the electrodes, because the porosity varies during charge and discharge. This variation is characterized by the maximum active surface area a_{max}, and the Morphology number (dimensionless). The equation of active surface area during discharge is shown in Equation (3.21):

$$a_ʊ = a_{ʊ,max}\left(\frac{\varepsilon - \varepsilon_0}{\varepsilon_{max} - \varepsilon_0}\right)^{\xi} \quad (3.21)$$

where ξ is a morphology correction number (dimensionless). Moreover, this active surface area can be measured to understand the side reactions that are oxygen evolution and reduction, and the non-faradaic double layer currents.

The following active surface area equation for the charging reactions is needed since $PbSO_4$ decreases the available active surface area due to the fact that $PbSO_4$ is an insulator as well as a reactant.

$$a_{ʊ,charge} = a_{ʊ,max}\left(\frac{\varepsilon - \varepsilon_0}{\varepsilon_{max} - \varepsilon_0}\right)^{\xi}\left(\frac{\varepsilon_{max} - \varepsilon}{\varepsilon_{max} - \varepsilon_0}\right) \quad (3.22)$$

3.7. Equations Governing Modes of Mass Transfer

Nernst-Planck equation covers mass transport of species including diffusion, migration, and convection.

3.7.1. Nernst-Planck Equation

A lead acid battery has two zones which are solid and liquid zones. The solid zone includes the anode electrode and the cathode electrode, but also there is some liquid in these electrodes. They are known as the porous electrodes as explained in previous sections. The liquid zone is the electrolyte. For the lead acid battery, mass transport is an important factor both the solid part and the liquid part calculated is expressed by the Nernst-Planck equation. The mass transport equation is used for electrolyte; it is also used for the porous electrode since it also has electrolyte. In order to explain the charge transport in electrodes, Ohm's law is an effective solution. While describing the charge and mass transport in the electrolyte, concentrated electrolyte theory is employed. Mass transport causes the change in state-of-charge in porous electrode due to the porosity (Boovaragavan, Methakar, Ramadesigan, & Subramanian, 2009). When Ohm's law is utilized to determine the flow of current in electrodes providing charge balance, Nernst-Planck equation determines transport of charged and neutral species in the electrolyte. The mass transport is provided by three ways which are diffusion, migration, and convection of ions. Diffusion is valid for all ions, but migration only occurs when an electric field exists.

$$\mathrm{E} = \frac{\partial \Phi}{\partial \mathrm{x}} \ (\mathrm{V/m}) \tag{3.23}$$

Equation (3.23) is applied to the Fick's first law Equation (3.2), thus, the general Nernst-Planck equation is obtained written as Equation (3.24).

$$\mathrm{J_i} = -\mathrm{D_i}\frac{\partial \mathrm{c_i}}{\partial \mathrm{x}} + \mathrm{z_i c_i D_i}\frac{\mathrm{F}}{\mathrm{RT}}\mathrm{E} \tag{3.24}$$

In addition, when the battery is flow battery or there is any force convection, mass transport by convection is added to Equation (3.24):

$$\mathrm{J_i} = -\mathrm{D_i}\frac{\partial \mathrm{c_i}}{\partial \mathrm{x}} + \mathrm{z_i c_i D_i}\frac{\mathrm{F}}{\mathrm{RT}}\mathrm{E} + \mathrm{C_i u} \tag{3.25}$$

where J_i is flux of species i (mol/cm^2.sec), z_i is charge number of ionic species i (dimensionless), u is the electrochemical or mechanical mobility (cm^2/V.sec), c_i is concentration of species i (mol/cm^3), D_i is the diffusion coefficient of species i (cm^2/sec).

To sum up, in the Nernst-Planck equation, the first term, the second term, and the third term represent diffusion, migration, and convection transport, respectively. The migration has a significance in terms of charge of the species and the value of electric field gradient (Brett & Brett, 1993). In our model, the third term is negligible, because there is no bulk motion and LA battery modeled in this study is not a flow battery. In this way, the mass transport in this study is just related to diffusion.

According to Ohm's law, current can be expressed as;

$$I = \frac{V}{R} \tag{3.26}$$

Current is the derivative of charge with respect to time in Equation (3.27).

$$I = \frac{dQ}{dt} \tag{3.27}$$

Current density is known as Equation (3.28).

$$i = F \sum_i z_i J_i \tag{3.28}$$

However, if concentration variation is neglected, the other current density can be expressed as;

$$i = -k\Delta\phi \tag{3.29}$$

where k is the conductivity shown in Expression (3.30).

$$k = F^2 \sum_i z_i^2 u_i c_i \tag{3.30}$$

The concentration is an important factor for electrolyte, thus by adding the concentration parameter; Ohm's law becomes;

$$\nabla\phi = \frac{-i}{k} - \frac{F}{k}\sum_{i} z_i D_i \nabla c_i \tag{3.31}$$

When Equation (3.28) is written into Equation (3.25), Equation (3.32) is obtained.

$$i = -F\sum D_i z_i \nabla c_i - \frac{F^2}{RT}\nabla\phi \sum z_i^2 D_i c_i + u\sum z_i c_i \tag{3.32}$$

Nernst-Planck equation just gives the information about the position of equilibrium of the reaction. Tafel and Butler-Volmer equations come into play to give more insight about the kinetics and current generation. These equations give the current density due to the electrochemical reaction as a function of the overpotential, the concentration of the reactants and the products. While Tafel equation explains an irreversible anodic-cathodic process, Butler-Volmer defines a reversible anodic or a cathodic process. The Tafel equation is written below as;

$$\log\left(\frac{i}{i_0}\right) = A\eta \tag{3.33}$$

where η is the overpotential (V) that is equal to;

$$\eta_m = \phi_s - \phi_l - E_{eq,m} \tag{3.34}$$

where ϕ_s (V) is the electrode potential, ϕ_l (V) is the electrolyte potential. In the Tafel Equation (3.33), A is the constant expressing the Tafel slope (1/V), i_0 is reference exchange current density. This shows that the definition is the current density described at zero overpotential. Yet, the current flow for Butler-Volmer equation relies on the magnitude and sign of overpotential:

$$i = i_0 \left(\exp\left(\frac{\alpha_a F \eta}{RT}\right) - \exp\left(\frac{-\alpha_c F \eta}{RT}\right) \right) \tag{3.35}$$

where α_a is the anodic transfer coefficient (dimensionless), α_c is the cathodic transfer coefficient (dimensionless). Equation (3.35) is the most general description of electrode kinetics. If a reversible reaction has really low overpotential (η of order RT/F ~ 25 mV), the exponential terms can be transformed as linear in Butler-Volmer equation:

$$i_{loc} = i_0 \left(\frac{(\alpha_a + \alpha_c)F}{RT} \right) \eta \tag{3.36}$$

where i_{loc} is local current density (A/m^2) at the electrode-electrolyte interface depend on the overpotential.

Furthermore, Tafel Law and Butler-Volmer equation determine the amount of the current because of the electrolysis. This current is the Faradaic current. There is also capacitive current, due to the attraction or repulsion of ions. The electrode kinetics is associated with the electrolyte concentration defined by Butler-Volmer equation the following expression:

$$i_{loc} = i_0 \left(\frac{c_l}{c_{l,ref}} \right)^{\gamma} \left(\exp\left(\frac{\alpha_a F \eta}{RT}\right) - \exp\left(\frac{-\alpha_c F \eta}{RT}\right) \right) \tag{3.37}$$

where γ is the reaction order (dimensionless), c_l is the dissociated salt concentration of electrolyte.

The double layer consists of layers of charge and opposite charge on the electrode and in the adjacent electrolyte, respectively. It acts as a parallel layer capacitance. In order to figure out a constant ideal capacitance across the electrode-electrolyte interface, the simple empirical method illustrates the observed influence of capacitance on polarization curve. The capacitor keeps a surface charge density given in Equation (3.38);

$$Q = C_d(\phi_s - \phi_l) \tag{3.38}$$

and helps a dynamic charging current density (non-Faradaic current);

$$i_{NF} = dQ/dt \tag{3.39}$$

The total current obtained from a real experiment is equal to Equation (3.40).

$$i_{tot} = i_{Far} + i_{NF} \tag{3.40}$$

Porosity in separator (ε_{sep}, dimensionless), and the exponent on porosity in electrolyte (ex, dimensionless) must be also taken into account. When considering mass balance situation, the electrode volume fraction (ε_s), and the electrolyte volume fraction ε_l are employed to determine the available volume of each phase in the mass balance equation, and in order to find surface area in the porous electrode reaction.

CHAPTER 4

RESULTS OF GRID MODELING

The grids' geometry of SLI, stationary and traction batteries are usually rectangular. Examples of grid geometries are given by Figure 4.1. A grid consists of perpendicular and horizontal wires that are the current collector covered by a thicker frame. The lug serves as carrier of the current to/from the grid. The grid design for the commercial lead-acid batteries are made in various forms which are conventional plate, expanded metal, tubular, and fiber types (Jung et al., 2015).

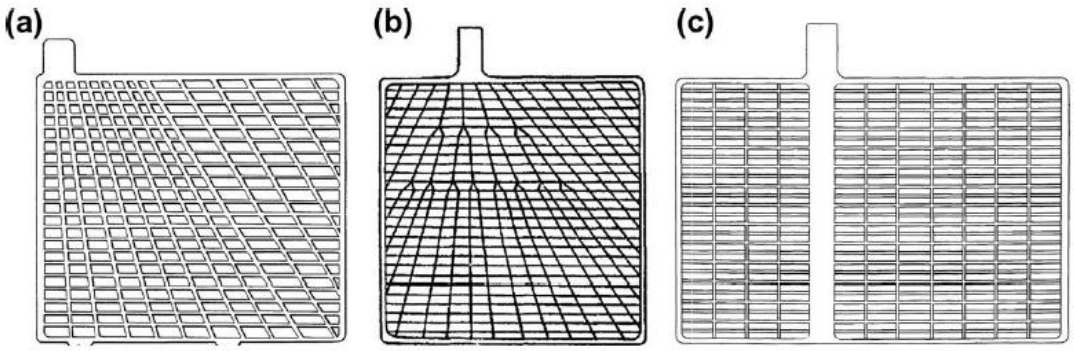

Figure 4.1. Rectangular grids (a,b) with diagonal wires directed to the lug and (c) with a vertical lug crossing the grid from bottom to top and conducting (collecting) the current from the horizontal wires (Source: Pavlov, 2011).

Negative plate thicknesses of SLI battery are between 1 and 1.4 mm while positive plate thicknesses vary between 1.2 and 1.8 mm. The thicknesses of heavy-duty batteries is between 1.6 and 2.25 mm. Traction batteries are thicker than both SLI and heavy-duty batteries due to the requirement of advanced cycling ability.

A lead acid battery consists of two grid plates that hold the positive and negative active masses. These active materials go through expansion and narrowing during discharge and recharge, respectively. While designing a grid, good electrical and mechanical contact should be taken into consideration between the grid surface and the active material. Since all the grid materials have internal resistances, a potential drop is observed during discharge. Therefore, the grid wire design should be optimized to minimize the potential drop. Moreover, the uniform current distribution and the

electrochemical reactions at a uniform rate can be obtained by the optimum plate design.

Grid design generally requires that the wire density is more intense near the lug (Pavlov, 2011). More vertical lines are required closer to the lug in order to obtain more the uniform current and potential distributions by shortening of the pathway for current transport from grid plate to the lug. Therefore, one can assume that a lug located in the middle of the grid should be better for battery performance; however, connecting several cells in series and cost issues usually prohibits this. Several different grid designs are shown in Figure 4.2.

Additionally, grid weight has an impact on the grid performance. The potential distribution becomes more uniform while increasing the grid weight. Yet, this increases the production cost of a battery. One must keep the weight at minimum without reducing the current collecting ability of the grid. A few studies in literature focused on grid design with respect to current and potential distribution. For example, grid design was modeled in order to measure the effects of a variety of grid configurations on resistive potential loss in battery plates by Sunu and Burrows in 1982 (Sunu & Burrows, 1982). Later, grid design was improved by Kao and Mrotek in 1996 with minimum weight and maximum battery performance (Mrotek, Kao, & Deer, 1996).

The grids in LA batteries may be corroded in time. Also, the positive and negative plates are converted from PbO_2 to $PbSO_4$ and from Pb to $PbSO_4$ during discharge, respectively. In the course of the transformation, the expansion occurs in the positive plate; then the grid should hinder the expansion forces while keeping the active material. Since the positive grid is subjected to corrosion, the grid needs to preserve its shape, so it should be thick as much as possible. However, this is not possible due to weight and cost problems; therefore, the optimum weight should be determined based on the value of a dimensionless weight parameter, α:

$$\alpha = \frac{W_g}{W_g + W_{am}} \tag{4.1}$$

where W_g and W_{am} (N) are grid and active mass, respectively. Ideally, the ratio of α should vary between 0.35 to 0.6 (Pavlov, 2011).

Another parameter for the performance is the surface area of the active materials of the electrodes. Because the negative and positive electrodes generate Pb^{+2} ions when reacting with H_2SO_4 in the course of the turning into $PbSO_4$ on the surface of the active materials, the electrodes become ineffective. Power output of the battery is reduced, as the active materials have reduced surface area due to surface passivation. Therefore, the surface area of the active masses should be increased (Pavlov, 2011). The surface parameter, ɣ (g/cm^2), is determined by the ratio of the weight of PbO_2 (W_{PbO2}) to the grid surface area (S_{grid});

$$\gamma = \frac{W_{PbO2}}{S_{grid}} \tag{4.2}$$

The value ought to be less than 1 g/cm^2 for good battery performance. Lower ɣ can lead to accelerated grid corrosion and short cycle life while higher values increase the weight and cost of the battery. Therefore, using alloys for the grid is a good alternative to increase corrosion resistance without weight penalty (Jung et al., 2015).

4.1. Grid Modeling

As mentioned previously, the grid design is important for the performance of lead-acid battery.

Potential drop and the current distribution non-uniformity result from internal resistance of the grid components. An optimized grid design is necessary for the minimum potential drop and the uniform potential and current distribution, which leads to better battery performance. Grid models used in this study contain two materials (electrode and electrolyte materials) and two domains. The solid domain, which is made of electrode material, is called the solid electrode. The liquid domains are electrolyte and a porous electrode which contains solid electrode material mixed with a liquid electrolyte. The grid consists of a solid electrode pasted with a porous electrode, and a lug to transmit the current. In addition, there is a pure electrolyte domain behind the grid. In the model, volume fraction was assumed 0.5 for porous electrode. Electrolyte made of sulfuric acid has a conductivity as 90 S/m at initial concentration. For simplification, the negative electrode was assumed to be pure lead. A grid is 11.4 cm in height and 14.4 cm in width corresponding to a 164.16 cm^2 cross-sectional area for the

electrolyte domain (with 1.76 mm in thickness) behind it. The thickness of the grid was 1.6 mm. The density of electrode material as taken as 11.34 g/cm^3. Table 4.1 lists various grid designs and calculated α parameters.

Table 4.1. Weight, volume and α parameters for various grid geometries.

Grid Name	Grid Weight (N)	Active Mass Weight (N)	Grid Volume (cm^3)	Active Mass Volume (cm^3)	α
Grid 1	0.8768	2.0448	7.89	18.4	0.30
Grid 2	1.0734	1.8447	9.66	16.6	0.36
Grid 3	0.7945	2.1226	7.15	19.1	0.27
Grid 4	0.8168	2.1003	7.35	18.9	0.28
Grid 5	0.8757	2.0448	7.88	18.4	0.29

Computer Aided Design (CAD) together with various numerical tools for modeling and simulation of engineering products can help grid design optimization without fabrication and testing, thus saving time and reducing cost. The popular numerical methods are finite element method (FEM) or analysis (FEA), finite volume method (FVM) and finite difference method (FDM).

For grid modeling, FEA method was used. A 3D grid of lead acid cell was generated to determine potential and current distribution of five different grid geometries. The potential and current distributions in solid and porous electrode domains were calculated by using fundamental equations given below and previous sections. For the simulation, 100 A was applied orthogonal to the lug and the equilibrium potential of the electrode was assumed as 1.76 V.

While modeling an electrochemical cell, three current distributions, primary, secondary and tertiary, are considered. In these distributions, the different approaches exist that depend on the relative significance of solution resistance, finite electrode kinetics, and mass transport.

Internal resistance of the grid leads to a potential drop and a non-uniform current density distribution based on the geometry of the electrode. Other factors can be listed as;

- The conductivity of electrolyte
- Activation overpotential depends on electrode kinetics
- Concentration overpotential depends on mass transport of the reactants
- Mass transport of ions in the electrolyte
- The operating conditions

Ideally, the potential and current density in the electrodes and the electrolyte must be determined by taking into account all of the parameters given above. Moreover, the contribution of species concentrations and the electrolysis (Faradaic) reactions can also be evaluated. According to the basic theory, Ohm's law shown in Equation (4.3) manages the current and potential relation in the electrodes:

$$i_s = -\sigma_s \nabla \phi_s \tag{4.3}$$

with Equation (4.4) of the conservation of current.

$$\nabla . i_s = Q_s \tag{4.4}$$

The current density in the electrolyte is calculated with Equation (4.5).

$$i_l = F \sum_i z_i J_i \tag{4.5}$$

Equations (4.3) and (4.5) have been described in Chapter 3 in detail.

The Nernst-Planck equation mentioned in Chapter 3 is related to the flux of an ion in an electrolyte solution and covers transport by diffusion, migration, and convection. By substituting the Nernst-Planck equation into Equations (4.5) and (4.6) current density can be obtained. All these equations are solved by taking into account the conservation of current in the electrode and electrolyte. In addition, one must pay attention to the interface between the electrode and the electrolyte and, the current must be conserved in here, as well. There are two ways to transmit the current between the electrode and the electrolyte domains which are Faradaic current by the electrochemical

reactions and non-Faradaic current by dynamic charging or discharging of the charged double layer of ions adjacent to the electrode. Primary current distribution (PCD) and secondary current distribution (SCD) differs on how the electrode reactions occur at interfaces of electrodes and electrolytes. While PCD applies Dirichlet boundary condition due to potential constraints, SCD uses Neumann boundary conditions owing to current flux conditions with regard to the equilibrium potential and the sum of the current densities of all electrode reaction, respectively.

4.1.1. Dependent Variables

Primary and secondary current distributions have two dependent variables, the electrolyte potential and the electric potential for the electrode. The current is transmitted by ions in the electrolyte; on the other hand, the electrons provide the current transportation in the electrode.

4.1.2. Domain Equations for Primary and Secondary Current Distributions

The domain equations will be explained below for PCD and SCD. The current flow mentioned previously by Equation (4.6) becomes a simple current density equation by neglecting the convection due to the electroneutrality and the diffusion term because the electroneutral solution does not induce the current flow and the gradients of the charge carrying species are assumed as zero. Therefore, the current density vector in an electrolyte can be written as;

$$i = -F\sum D_i z_i \nabla c_i - \frac{F^2}{RT}\nabla\phi \sum z_i^2 D_i c_i + u\sum z_i c_i \tag{4.6}$$

$$i_l = -F^2 \sum z_i^2 u_{m,i} c_i \nabla\phi_l \tag{4.7}$$

After that, the current density vector can be shown Equation (4.9) with a constant electrolyte conductivity defined with Equation (4.8).

$$\sigma_l = F^2 \sum z_i^2 \, u_{m,i} c_i \tag{4.8}$$

$$i_l = -\sigma_l \nabla \phi_l \tag{4.9}$$

In addition, the equation of conservation of charge governs the domain equation of Primary and Secondary Current Distribution for the electrolyte as shown below in Equation (4.10).

$$\nabla . \, i_l = 0 \tag{4.10}$$

While evaluating current conduction of the solid electrode, the Ohm's law is applied;

$$\nabla . \, i_k = Q_k \tag{4.11}$$

$$i_k = -\sigma_k \nabla \phi_k \tag{4.12}$$

where Q_k, k, σ_k, and ϕ_k indicate a general source term, an index l for the electrolyte and s for the electrode, the conductivity (S/m) and the potential (V).

Even though the primary and secondary current distribution interfaces use Ohm's law to deliver current with a constant conductivity, there is a difference between the interfaces of an electrolyte and an electrode according to the electrochemical charge transfer reaction. While PCD neglects the electrochemical reactions of kinetics, that is, when there is no activation overpotential, SCD considers overpotential by measuring the electrochemical reactions. Besides, SCD uses the equations of the charge transfer and overpotential, for instance, in the Butler-Volmer and Tafel equations.

In this model, current distribution was determined based on solution resistance, neglecting electrode kinetic and concentration dependent effects. One of the assumptions is electroneutrality, this causes omission of the convective contribution to the current density in Equation (4.6). The other one is the composition variation that is homogeneous in the electrolyte. The transport of charged ions in an electrolyte of uniform composition and current conduction in the electrodes (by utilizing Ohm's law

in combination with a charge balance) were modeled. Additionally, lack of the activation overpotential was assumed owing to charge transfer reactions. Furthermore, the ohmic losses in simplified models of grids were determined, where the overpotential of the electrode reactions are small compared to the ohmic potential drops in the electrolyte and electrodes.

Consequently, the equations used in the model are listed below in Equations (4.13), (4.14), and (4.15).

Electrode: $$i_s = -\sigma_s \nabla \phi_s \text{ with } \nabla . i_s = Q_s \quad (4.13)$$

Electrolyte: $$i_l = -\sigma_l \nabla \phi_l \text{ with } \nabla . i_l = Q_l \quad (4.14)$$

Electrode-Electrolyte-Interface: $$\phi_s - \phi_l = E_{eq,m} \quad (4.15)$$

Comparing these five grid geometries, non-uniform wire design gives us more effective current collection ability in grid, unlike uniform wire design. Grid 2, 3, 4 and 5 have non-uniform wire distribution with lower ohmic resistance, whereas grid 1 has uniform wire design.

Grid 4 and grid 5 have novel geometries, whereas grid 1, grid 2, and grid 3 are taken from the literature (Nakhaie, Benhangi, Alfantazi, & Davoodi, 2014).

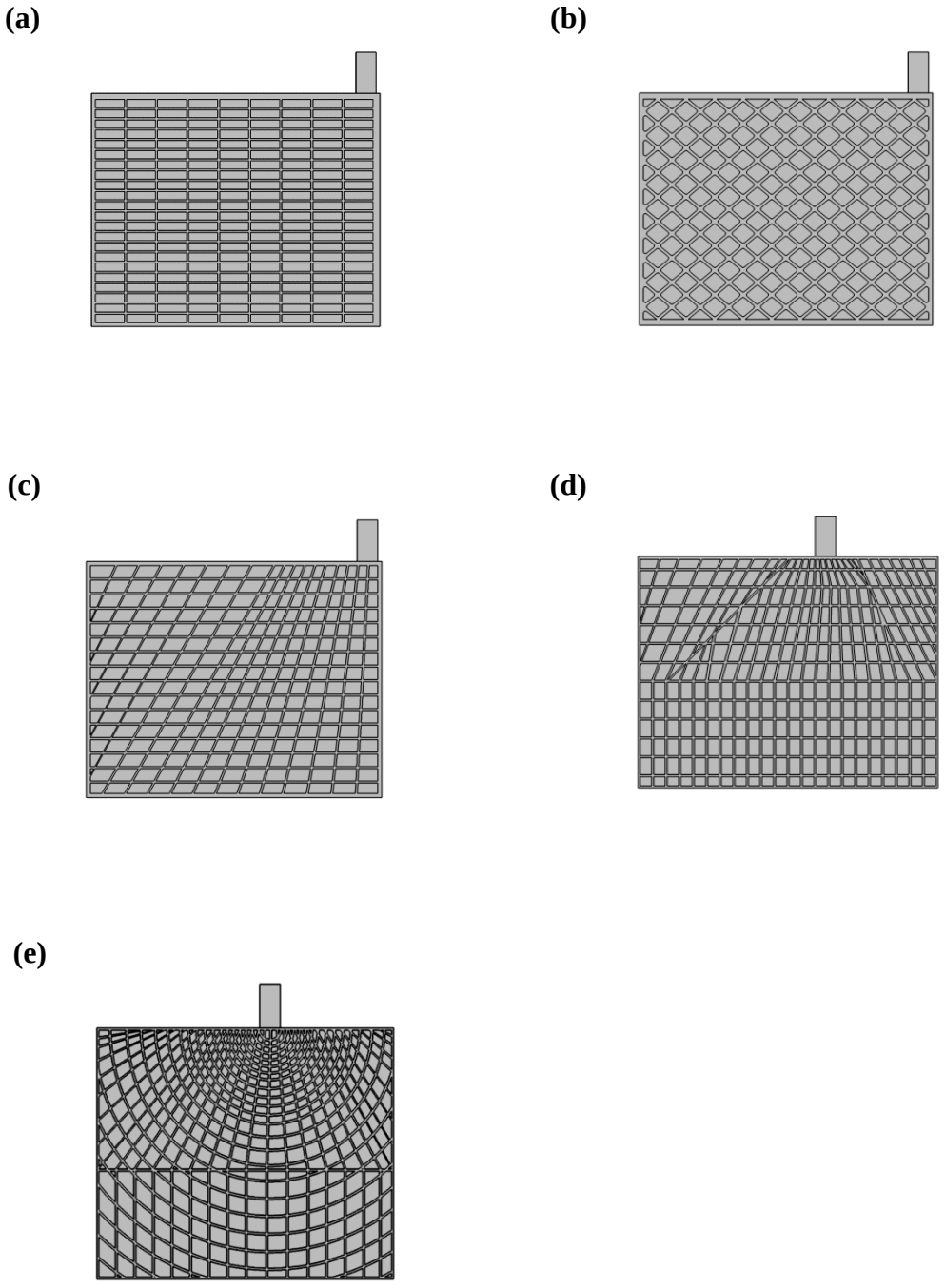

Figure 4.2. A schematic of five different grid configurations applied to the model; (a) Grid 1, (b) Grid 2, (c) Grid 3, (d) Grid 4, (e) Grid 5.

4.2. Potential Distribution of the Grids

Figure 4.3 shows that the potential distribution in porous electrodes (including solid frame and porous domains). While comparing all five geometries, the lowest potential drop was obtained from grid 4, whereas the highest potential drop was seen in grid 1.

Minimum and maximum potential values obtained for different grid geometries are listed in Table 4.2. It should be noted that when different current density values were used in the model, still similar results were obtained. Grid 1 always showed approximately 1.4 times more potential drop than best performing Grid 4.

The better results are usually seen in non-uniform wire design; this paves the way for better current distribution and lower potential drop in the grid. When the wire density is high, more uniform potential distribution is observed. Therefore, grid 4 has the best current collecting ability. The wire density should be higher near the lug, since current density is highest around the lug. The current density starts to fall from the lug to the bottom.

Consequently, while designing a battery grid, the lug should be positioned at the midpoint, the vertical wire should be more frequent near the lug so as to shorten the path of the current and, provide more uniform the potential distribution. The size of the grid, thickness, wire size, active material fraction and porosity all play important roles for grid performance. However, the cost and weight should also be taken into account since better performing grids does necessarily translate into economically feasible products.

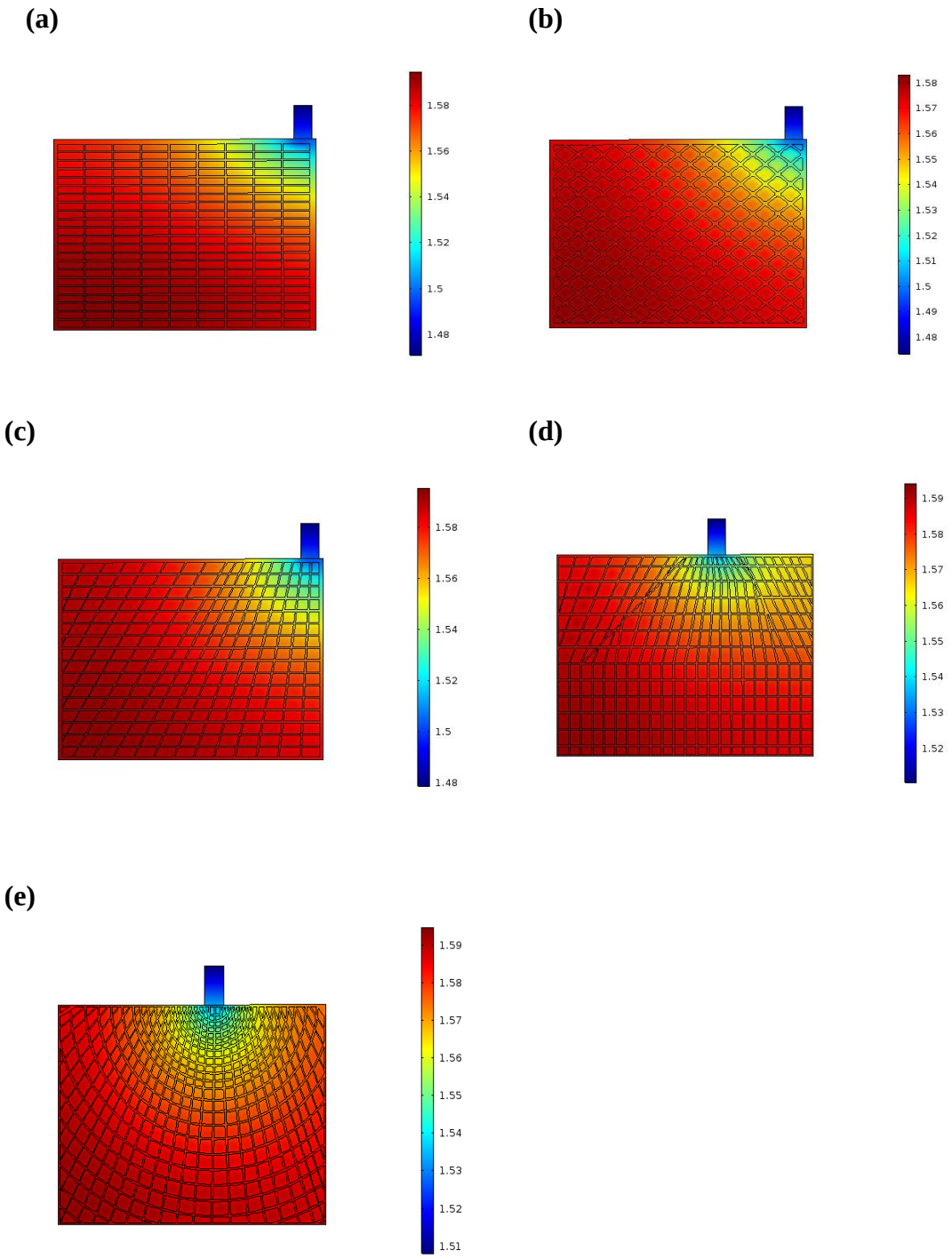

Figure 4.3. Potential Distribution (V) of Solid and Porous Electrode; (a) Grid 1, (b) Grid 2, (c) Grid 3, (d) Grid 4, (e) Grid 5.

Table 4.2. Maximum and minimum values for Grid 1, Grid 2, Grid 3, Grid 4 and Grid 5.

Grid name	E_{max} (V)	E_{min} (V)	Potential Difference (mV)
Grid 1	1.594	1.471	123
Grid 2	1.583	1.473	110
Grid 3	1.595	1.478	117
Grid 4	1.594	1.510	84
Grid 5	1.596	1.506	90

4.3. Potential Distribution of Solid Electrode

In Table 4.2, Grid 4 seems the best among the other models while Grid 5 differs from the others with respect to wire geometry; it has the radial wire design. To our knowledge, no gird with radial wire geometries has been used commercially. Table 4.2 lists potential drops when entire grid volume was taken into account. If the potential drop only in the solid frame (solid electrode) is calculated, different potential drops, but still a similar behavior is seen. As expected slightly lower potential drops were obtained since porous active material has slightly higher resistivity compared to solid material. However, the performance of grid can be altered significantly by changing the wire size, the thickness of the grid and the volume fraction of the porous active material. This in turn will change the weight and fabrication cost. Therefore, one must not rely on one test or simulation result to determine the best grid geometry.

Table 4.3. Maximum and minimum potential values of solid electrodes for Grid 1, Grid 2, Grid 3, Grid 4, and Grid 5.

Grid name	**E_{max} (V)**	**E_{min} (V)**	**Potential Difference (mV)**
Grid 1	1.592	1.471	121
Grid 2	1.577	1.473	104
Grid 3	1.591	1.478	113
Grid 4	1.590	1.510	80
Grid 5	1.592	1.506	86

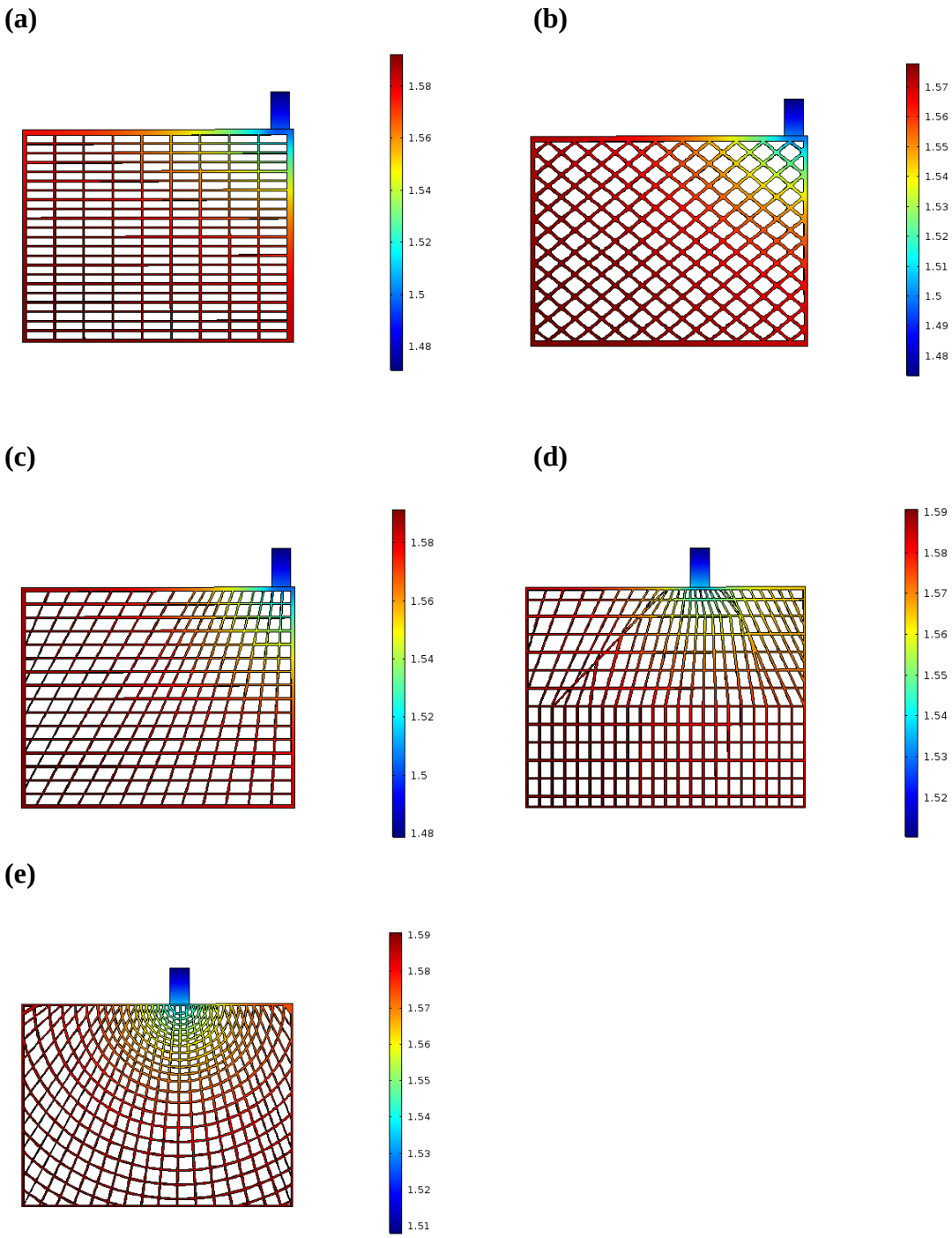

Figure 4.4. Potential Distribution (V) of Solid Electrode; (a) Grid 1, (b) Grid 2, (c) Grid 3, (d) Grid 4, (e) Grid 5.

4.4. Potential Distribution of Porous Electrode and Adjacent Electrolyte to the Grid

The difference of the potential distribution of active material and the electrolyte was determined to be minimum in Grid 4. In this analysis, electrolyte outer surface except the back boundary of electrolyte domain and the outer boundaries of grid and lug are specified as insulators, so their potential values are assumed to be zero. Figure 4.5 shows potential value increases from the negative value from the left corner of the grid to zero to near the lug. In addition, Table 4.4 lists the value of maximum and minimum potentials. Similar to previous analysis, Grid 4 is the best performing grid geometry when all other parameters are kept constant.

Table 4.4. Maximum and minimum potential values of active material and adjacent electrolyte to the grid in case of five different geometries; Grid 1, Grid 2, Grid 3, Grid 4, and Grid 5.

Grid name	E_{max} (V)	E_{min} (V)	Potential Difference (mV)
Grid 1	0	-0.202	202
Grid 2	0	-0.199	199
Grid 3	0	-0.194	194
Grid 4	0	-0.163	163
Grid 5	0	-0.167	167

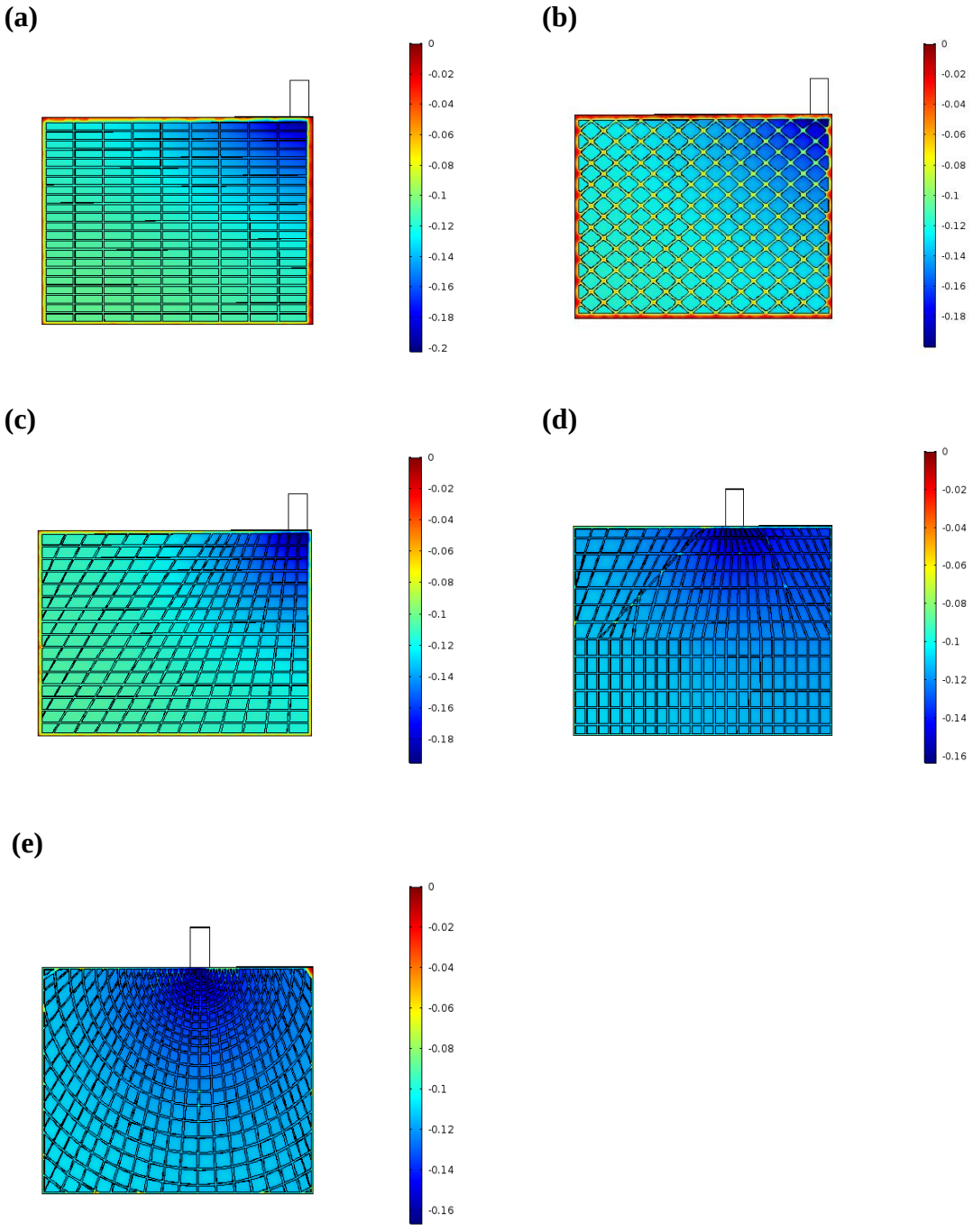

Figure 4.5. Potential distribution (V) of porous electrode and adjacent electrolyte to the grids; (a) Grid 1, (b) Grid 2, (c) Grid 3, (d) Grid 4, (e) Grid 5.

4.5. Current Density Distribution

The current distribution can be improved with some important design methods mentioned in Grid Design section. Since all current passes through the lug, the more vertical line should be placed in the direction of the lug; also, the lug can be set in the middle of the upper of the grid. In Figure 4.6, the current density reduces from the lug to the bottom of the grid plate due to the ohmic resistance of the electrolyte. Comparing five geometries, the design of Grid 5 has the most uniform current density. According to Ohm's law, at a constant resistance, while increasing potential, current reduction is observed. Therefore, Figure 4.6 verifies potential drop and current drop results.

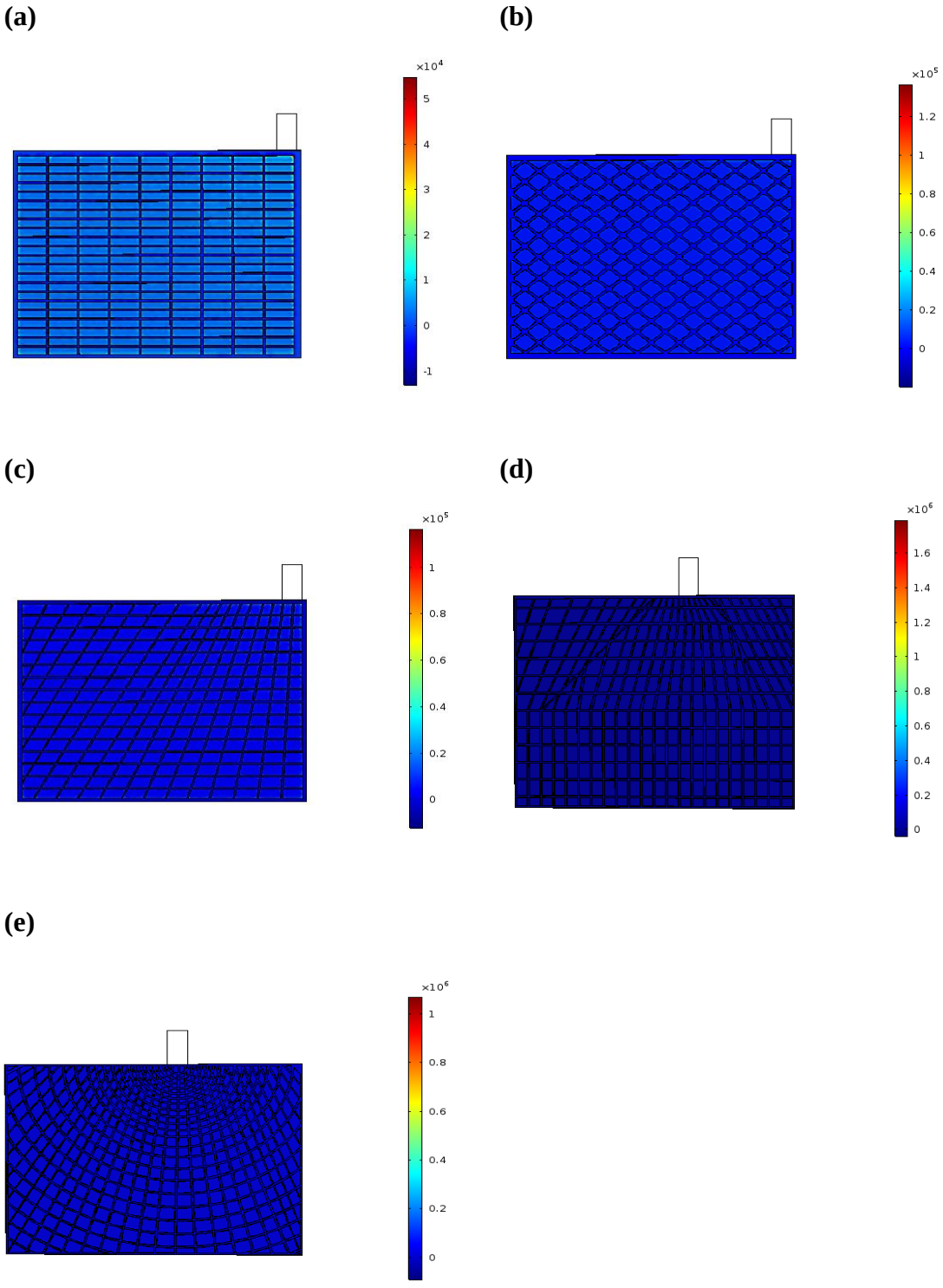

Figure 4.6. Distribution of current density (A/m2) in the electrolyte adjacent to surface of each grid with different configurations; (a) Grid 1, (b) Grid 2, (c) Grid 3, (d) Grid 4, (e) Grid 5.

CHAPTER 5

RESULTS OF LEAD-ACID CELL MODEL

In literature, the lead acid cell modeling started with Stein in 1958-1959, and Euler in 1961 (H. Gu & Nguyen, 1987). They used a positive porous electrode (PbO_2) to understand the behavior of the lead-acid cell. After that, Simonsson, Micka and Rousar, Gidaspow and Baker in 1973 continued to work on porous media modeling. Later, Tiedeman and Newmann studied the theory of flooded porous electrodes (Newman & Tiedeman, 1975). In the following years, Tiedemann and Newman in 1979, and Sunu in 1984 provided a complete battery model for the discharge behavior of the lead-acid battery using Newman's theory; however, those studies were not enough to understand the battery behavior during charge and rest completely. A more advanced mathematical model of a lead acid battery was needed to predict its behavior during charge and rest as well as during discharge. The model of Gu et al did not presented detailed non-uniformities along cell height although it gave the good results when the thickness and porosity of electrodes and separator were changed. In addition, Gu et al examined a lead acid cell model that includes free convection resulting from density variations because of acid stratification as well as electrochemical kinetics and mass transport (W. B. Gu, Wang, & Liaw, 1997). Bernardi et al presented a mathematical model in 1993 (Bernardi, Gu, & Schoene, 1993) and more recently, the behavior of flooded battery in all vehicle life cycle was studied by Cugnet et all (Cugnet et al., 2009).

In the lead-acid battery, the side reactions take place as well as main electrochemical reactions during the discharge and charge reactions. The side reactions take place in positive and negative electrodes.

Electrochemical reaction in the positive electrode ($PbO_2/PbSO_4$):

$$PbSO_{4(s)} + 2H_2O \underset{discharge}{\overset{charge}{\rightleftharpoons}} PbO_{2(s)} + HSO_4^- + 3H^+ + 2e^- \tag{5.1}$$

with oxygen evolution:

$$2H_2O \rightarrow O_2 + 4H^+ + 4e^- \quad (5.2)$$

hydrogen recombination:

$$H_2 \rightarrow 2H^+ + 2e^- \quad (5.3)$$

Electrochemical reaction in the negative electrode ($Pb_{(s)}/PbSO_4$):

$$PbSO_{4(s)} + H^+ + 2e^- \underset{discharge}{\overset{charge}{\longrightarrow}} Pb_{(s)} + HSO_4^- \quad (5.4)$$

with oxygen recombination:

$$O_2 + 4H^+ + 4e^- \rightarrow 2H_2O \quad (5.5)$$

and hydrogen evolution:

$$2H^+ + 2e^- \rightarrow H_2 \quad (5.6)$$

with overall cell reaction:

$$2PbSO_{4(s)} + 2H_2O \underset{discharge}{\overset{charge}{\longrightarrow}} Pb_{(s)} + PbO_{2(s)} + 2H_2SO_4 \quad (5.7)$$

Equations (5.2), (5.3), (5.5) and (5.6) describe side reactions which show the internal oxygen and hydrogen cycles in the cell. There is a three-phase system in a VRLA cell because of the side reactions. The phase systems are the solid matrix, liquid electrolyte, and gas phase. First, oxygen is produced at the PbO_2/electrolyte interface. Later, oxygen is accumulated in gas phase when its solubility limit in the electrolyte is surpassed during operation. Oxygen gas can be dissolved in the electrolyte and be diminished at the Pb/electrolyte interface; therefore, the oxygen can be carried from the positive to the negative electrode by the liquid and gas phases. This is the internal oxygen cycle in VRLA cells. In addition, hydrogen is formed at the negative electrode, as given by Equation (5.6), when the electrode potential starts to drop. Further, hydrogen recombination at the positive electrode, as shown in Equation (5.3) (during the collection of oxygen and hydrogen in the gas phase), leads to venting due to the cell pressure built-up (W. B. Gu, Wang, & Wang, 2002). The start of discharge of a valve-

regulated lead-acid (VRLA) battery is based on two transient potential responses. One of them is related to battery's resistance and inductance. The second one is more complex than the first transient response because it is connected to the electrochemical reactions in the battery called as the 'coup de fouet' (Pascoe & Anbuky, 2002).

In this study, a simple 3D LA battery model based on grid geometries mentioned previously was used to evaluate simple discharge behavior. Although a 3D model is more complex and needs more computational power and time, a 3D model should give more accurate results and also provide time dependent potential, current density and concentration distributions in entire LA battery. In addition, porous electrode geometry effects can be also observed better.

Three-dimensional lead-acid cell model used in this study contains six domains: two porous electrodes, which are negative lead, and positive lead oxide porous electrodes, are connected to the negative electrode and the positive electrode, a separator, and an electrolyte as shown in Figure 5.1. The electrolyte transmits the current in the ion-conducting phase. The electrolyte comprises of sulfuric acid that is a binary electrolyte ($H^+$and HSO_4^-). Initial electrolyte salt concentration was assumed as 4900 mol/m^3, which is a typical value for commercial SLI batteries. The battery temperature was assumed to be constant during operation. The discharge current of 83 A was applied to orthogonal positive electrode grid lug.

The lead-acid battery models have been studied both experimentally and numerically for years; however, experimental methods are costly unpractical and time consuming. Therefore, numerical methods have gained considerable interest with the advance of computing technology. For 3D lead acid cell model, finite element analysis method was used with fundamental principles of thermodynamics, reaction kinetics, and transport theory. Hence, the potential drop and current density distribution calculated by FEM with a time-dependent solution at 298 K. The lead-acid cell was simulated at different discharge rates for 10 h and 44 h discharge time. In reality, LA batteries cannot be discharged below %80 SOC due to irreversible reactions (mainly sulfation) as explained in previous chapters. However, in order to evaluate the feasibility of the model, LA cells were discharged to a much lower SOC values in the simulation.

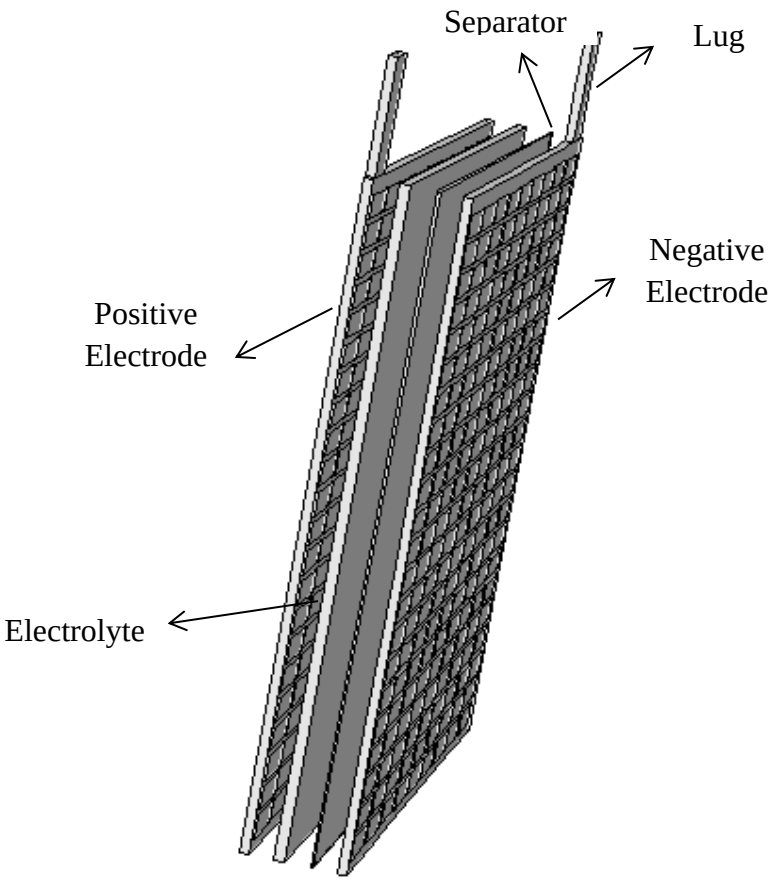

Figure 5.1. 3D LA battery model with Grid 1 geometry in electrodes.

No mass flux was assumed outside of boundaries which contains the electrolyte. The equation is shown below:

$$-n.N_l = 0 \tag{5.7}$$

The insulation condition is employed on the cell boundaries as shown in Equation (5.8).

$$-n.i_l = 0\,, -n.i_s = 0 \tag{5.8}$$

The reference electrode was selected as the negative electrode that has zero electric potential to calculate the potential difference. The thickness of electrodes, electrolyte and separator were assumed to be 1.6 mm, 1.76 mm, and 0.5 mm, respectively. The cell height, width, and thickness were 114 mm, 144 mm, and 5.46 mm, respectively. In addition, the height and width of lug were 20 mm and 10 mm,

respectively with the same cell thickness. In the model, Grid 1 geometry was used in both positive porous and negative porous electrodes.

Time dependent potential and current density distributions were calculated. The charge transport in the electrodes was calculated by Ohm's law, charge and mass transport in the electrolyte phase was calculated with concentrated electrolyte theory. The variation in the state of charge is due to mass balances for the porosities of the porous electrode. The electrode kinetics is determined by the Butler-Volmer equation based on the electrolyte concentration;

$$i_{loc} = i_0 \left(\frac{c_l}{c_{l,ref}}\right)^{\gamma} \left(exp\left(\frac{\alpha_a F \eta}{RT}\right) - exp\left(\frac{-\alpha_c F \eta}{RT}\right)\right) \tag{5.9}$$

where i_0, γ, α_a, and α_c indicate the exchange current density (A/m^2), the reaction rate (dimensionless), the anodic charge transfer coefficient (dimensionless) and the cathodic charge transfer coefficient (dimensionless), respectively. Also, the overpotential denotes with η, can be written as;

$$\eta = \phi_s - \phi_l - E_{eq} \tag{5.10}$$

The active surface area, a_v (m^2/m^3) during discharge and charge is determined from the following expression;

$$a_v = a_{v,max} \left(\frac{\varepsilon - \varepsilon_0}{\varepsilon_{max} - \varepsilon_0}\right)^{\xi} \text{ for discharge} \tag{5.11}$$

where ξ is a morphology correction parameter (dimensionless). Additionally, the surface area expression can be applied to side-reactions, which are oxygen evolution and reduction, and the non-faradaic double layer currents. Thus, porous matrix double layer capacitance can be added to calculate non-faradaic current density between the interface of the porous electrode and the electrolyte.

$$a_{v,charge} = a_{v,max} \left(\frac{\varepsilon - \varepsilon_0}{\varepsilon_{max} - \varepsilon_0}\right)^{\xi} \left(\frac{\varepsilon_{max} - \varepsilon}{\varepsilon_{max} - \varepsilon_0}\right) \text{ for charge} \tag{5.12}$$

$PbSO_4$ that is both a reactant and an insulator in the reactions of the charge decreases the available active surface area. Ohm's law is used to calculate the current

density of the electrode for the electrode charge transport in the electrode's current collectors and feeder:

$$i_s = -\sigma_s \nabla \phi_s \tag{5.13}$$

Moreover, porous electrode theory should be used to provide the current balance between a porous electrode domain and a pore electrode and mass balance of the electrolyte in a domain. In order to calculate the current density in porous electrode media, Equation (5.14) was employed. In this equation ε indicates the porosity of the electrode which is an empirical factor. The conductivities of the electrode and the diffusion coefficients of the electrolyte decrease due to tortuosity of the porous domain and the lower volume fractions of each phase. Therefore, the correction factor is utilized for the effective transport characteristics.

$$i_s = -\varepsilon^{exm} \sigma_s \nabla \phi_s \tag{5.14}$$

5.1. LA Battery Behavior

A battery has three main behaviors which are discharge, charge and float charge. During discharge operating phase, chemical energy is transformed to electrical energy whereas during charging the opposite happens. Battery's chemical energy level is kept in the float charge operating phase. The discharge, charge and float charge is a cycle to maintain battery life.

Discharge of a battery shows a complex behavior and depends on many factors such as ambient temperature, discharge rate, battery type, and initial SOC. First of all, as the discharge progresses, the potential reduces slowly. After that, decreasing potential starts to rise while discharge is still in progress. Therefore, the discharge potential reaches the "knee", later, it decreases swiftly. The next step is the end of the discharge. When the potential reaches the end voltage, the discharge process is over. The charge process initiates with a voltage higher than the open circuit voltage. When the battery potential comes the charge potential, the charge current reduces, this is called as the float charge phase (Pascoe & Anbuky, 2004).

5.2. The Potential in the Positive Electrode

In 3D lead-acid cell model, the positive plate discharge behavior was simulated in different C rates. C rate is a parameter used for quantifying charging and discharging rates, i.e., how fast or slow the charging and discharging processes are. At 1C, a battery is discharged fully in 1 hour, at 2C in 1/2 hours. Similarly, at 0.5C discharge rate, the battery will be fully discharge in 2 hours. Figure 5.2 shows discharge behavior for 11 hours at two C rates; 0.1C and 1C for a battery containing Grid 1 geometry at an ambient temperature of 298 K.

As seen on Figure 5.2, the discharge potential initially decreases slowly from 1.97 V to 1.92 V at 0.1C. After that, the discharge potential continues to drop very slowly for the entire simulation time. However, for 1C rate, the potential drops from 1.79 V to 1.75 V faster than the potential drop at 0.1C due to the high discharge current. The initial voltage at 0.1C is higher than the initial voltage at 1C due to high internal resistance. Small bump at 1 hour observed at 0.1C rate was not seen at higher discharge rate.

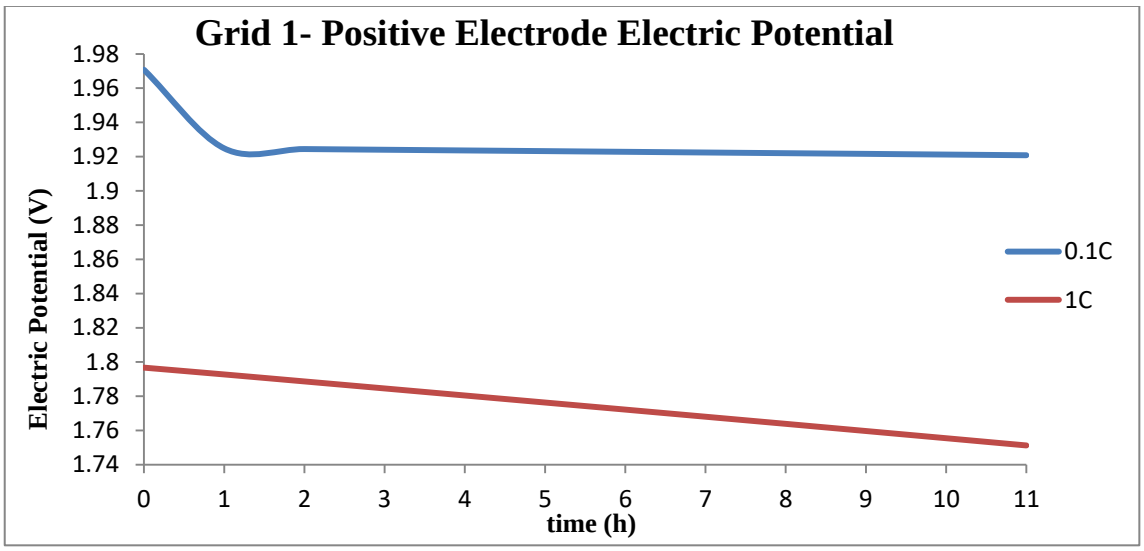

Figure 5.2. Positive electrode electric potential of LA battery with Grid 1 geometry at 0.1 C and 1 C discharge rates with 11 h discharge time.

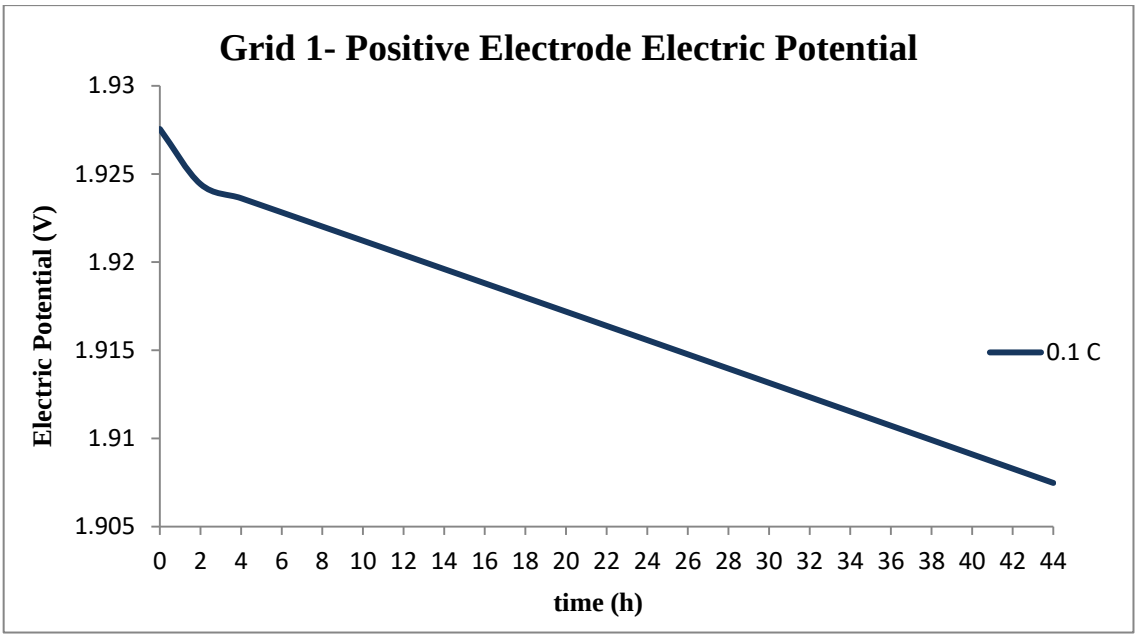

Figure 5.3. Positive electrode electric potential of LA battery with Grid 1 geometry at 0.1 C with 44 h discharge time.

The potential at the electrode decreases during discharging; therefore, we expect the potential drop in the two electrodes. However, due to difference of equilibrium potential of the positive and negative electrodes, the potential drop in positive electrode is less than 2.1 V cell potential. In the model, initial values were used to determine the potentials. When proper initial values are selected, solver convergence can be improved since non-linear electrode kinetics like Butler-Volmer kinetics is used in many electrochemical problems.

When comparing 3D model used in this study with 1D models employed widely in literature there are a few differences that needs to be taken into account. Due to geometry restrictions, a 1D LA battery model usually have more assumptions with respect to transport phenomena leading to less accuracy, but in return requires much less computational power and time. It is also very difficult to evaluate porous active domains in a 1D geometry. 3D model requires immensely higher computer power and time but in return give much more accurate results with fewer assumptions and simplifications. However, using a 3D model can make the parameter optimization more difficult due to increased complexity.

In 3D LA battery model, electrode current density, denoted as $i_{n,s}$, was equal to 83A at 1 C rate. Current density in the electrode was determined as different for each C rate from the following expression:

$$-n.i_s = i_{n,s} \tag{5.15}$$

Current density in solid electrode and in porous electrode was calculated by Equation (5.14). Current density as also calculated in electrolyte domain.

Figure 5.3 shows the discharge behavior of LA battery at 0.1 C rate for 44 hours. In 44 hours, the total potential drop was calculated to be around 25 mV. As expected smaller discharge rates will significantly reduce potential drop and the battery will last longer. At very high discharge current, the potential drop will increase dramatically and discharge time will be reduced.

Figure 5.4 shows positive electrode surface electric potential distribution at the start, in the middle and at the end of the simulation for 10 h and 44 h simulations times and at two different discharge rates.

The results show that 3D LA battery model provides reasonably accurate potential and current distribution although the results needs to be verified with experimental studies.

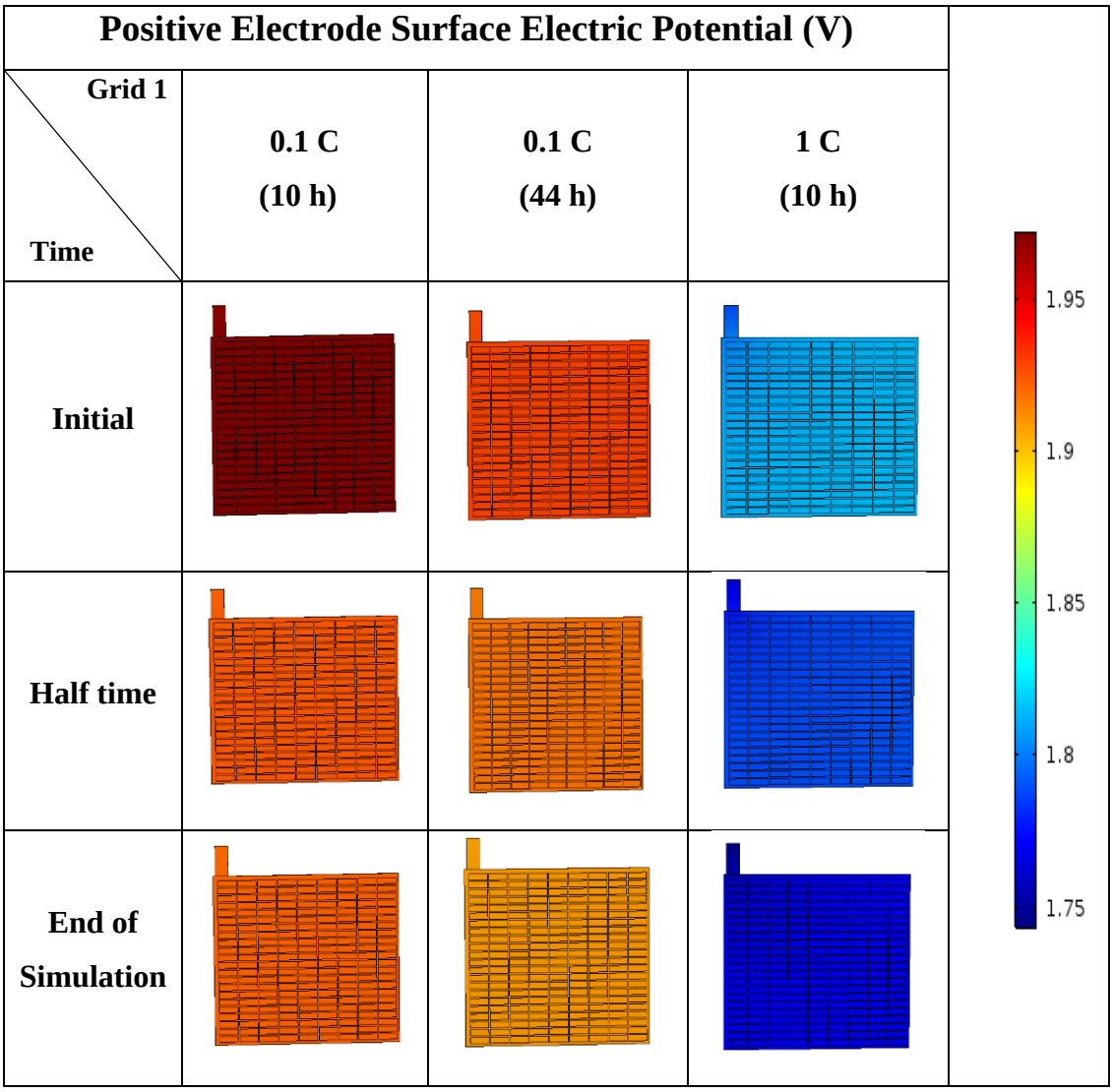

Figure 5.4. Surface electric potential distribution of positive electrode Grid 1 at two different C rates.

CHAPTER 6

CONCLUSION

This thesis aim was to evaluate performance of lead-acid battery different grid geometries. Optimization of the lead-acid battery cell's grid using a 3D mathematical model helps to obtain more uniform potential and current density distribution, while also keeping internal resistance at minimum. A total of five different grid geometries were used to evaluate potential drop and current density distribution. The optimum grid geometry was determined through the finite element analysis method. Numerical analysis and a mathematical model expressed battery behaviors under various conditions. Initially, the negative electrode of the lead-acid battery adjacent to the porous electrode was modeled three-dimensionally at the steady-state, using thermodynamics equations with minimum assumptions.

The distributions of the potential and current density were evaluated on both the solid electrode and the porous electrode. The optimum current collector battery grid was selected while addressing essential parameters. The non-uniform current and potential distributions were generally observed in non-symmetric grid designs. It was found out that increasing the wire density near the lug helps to reduce potential drop and at the same time increase current density uniformity. This necessitates using a non-symmetrical grid design and a lug ideally located near the middle of the top of the grid. However, for economical and ergonomically reasons, lug location in the middle might not be feasible. Increasing the density of vertical current collecting wires helps improving grid performance when the lug is not located in the middle.

Grid weight was found to be important parameter for optimum grid design. Therefore, it was concluded that the optimization of grid must take into account the following parameters: output current density, grid size, grid thickness, electrolyte concentration and conductivity, solid frame thickness and conductivity, porous domain fraction and conductivity, lug location, current collector wire size and density, and finally active weight.

Based on initial studies, discharge behavior of a LA battery cell was also evaluated using a 3D cell model under various discharge rates. As expected, it was

shown that high C rates lead to less capacity and high and fast potential drop. Longer discharge time and more uniform potential distribution and less potential drop were observed when lower discharge rates were employed. However, 3D model is not complete and needs improvement for accurate estimation of charge and discharge behavior.

With the advances in the computing technology, numerical modeling and evaluation of electrochemical energy storage technologies will help development of new battery electrodes and battery systems.

REFERENCES

Bernardi, D. M., Gu, H., & Schoene, A. Y. (1993). Two-Dimensional Mathematical Model of a Lead-Acid Cell. The Electrochemical Society Interface, 140(8), 2250–2258.

Besenhard, J. O. (1999). Handbook of Battery Materials. Weinheim: WILEY-VCH.

Boovaragavan, V., Methakar, R. N., Ramadesigan, V., & Subramanian, V. R. (2009). A Mathematical Model of the Lead-Acid Battery to Address the Effect of Corrosion. Journal of The Electrochemical Society, 156(11), A854–A862. http://doi.org/10.1149/1.3190510.

Brett, C., & Brett, A. (1993). Electrochemistry: Principles, Methods, and Applications. Midsomer Norton: Bookcraft (Bath) Ltd.

Calvo-baza, M. V., & Armenta-Deu, C. (1998). The Initial Voltage Drop in Lead – Acid Cells: The Influence of the Overvoltage. Journal of Power Sources, 72, 194–202.

Caris. (2014). History Of Batteries: A Timeline. Retrieved September 20, 2016, from http://www.upsbatterycenter.com/blog/history-batteries-timeline/#respond.

Cugnet, M., Laruelle, S., Grugeon, S., Sahut, B., Sabatier, J., Tarascon, J.-M., & Oustaloup, A. (2009). A Mathematical Model for the Simulation of New and Aged Automotive Lead-Acid Batteries. Journal of The Electrochemical Society, 156(12), A974–A985. http://doi.org/10.1149/1.3224868.

Cynthia G. Zoski. (2007). Handbook of Electrochemistry. Amsterdam: Elsevier. http://doi.org/10.1017/CBO9781107415324.004.

Dickinson, E. J. F., Limon-Petersen, J. G., & Compton, R. G. (2011). The electroneutrality approximation in electrochemistry. Journal of Solid State Electrochemistry, 15(7–8), 1335–1345. http://doi.org/10.1007/s10008-011-1323-X.

El-rahman, H. A. A., Salih, S. A., & El-Wahab, A. M. A. (2013). Electrochemical Performance of Grids of Lead-acid Batteries made from Pb-0.8%Ca-1.1%Sn Alloys Containing Cu, As and Sb Impurities in the presence of phosphoric acid. AFINIDAD LXX, 70 (564)(2339–9686), 295–304.

Ferg, E. E., Loyson, P., & Rust, N. (2005). Porosity measurements of electrodes used in lead-acid batteries. Journal of Power Sources, 141(2), 316–325. http://doi.org/10.1016/j.jpowsour.2004.09.018.

Garche, J. (1990). On the historical development of the lead/acid battery, especially in Europe. Journal of Power Sources, 31, 401–406.

Garche, J., & Dayer, C. K. (2009). Encyclopedia of Electrochemical Power Sources. London: Elsevier Science Technology.

Gu, H., & Nguyen, T. V. (1987). A Mathematical Model of a Lead-Acid Cell. Journal of The Electrochemical Society, 134(12), 2953–2960. http://doi.org/10.1149/1.2100322.

Gu, W. B., Wang, C. Y., & Liaw, B. Y. (1997). Transport Processes in Lead-Acid Batteries. The Electrochemical Society Interface, 144(6), 2053–2061.

Gu, W. B., Wang, G. Q., & Wang, C. Y. (2002). Modeling the overcharge process of VRLA batteries. Journal of Power Sources, 108(1–2), 174–184. http://doi.org/10.1016/S0378-7753(02)00043-5.

Hibbert, D. B. (1993). Introduction to Electrochemistry. London: The Macmillan Press Ltd.

Jung, J., Zhang, L., & Zhang, J. (2015). Lead-Acid Battery Technologies: Fundamentals, Materials, and Applications. Hoboken: CRC Press.

Kiehne, H. A. (2000). Battery Technology Handbook. Renningen-Malsheim: Expert Verlag.

Kurzweil, P. (2010). Gaston Planté and his invention of the lead-acid battery-The genesis of the first practical rechargeable battery. Journal of Power Sources, 195(14), 4424–4434. http://doi.org/10.1016/j.jpowsour.2009.12.126.

Linden, D., & Reddy, T. B. (2001). Handbook of Batteries. New York: McGraw-Hill.

M. Barak. (2006). Electrochemical Power Sources Primary and Secondary Sources. London: The Institution of Engineering and Technology.

Mrotek, E. N., Kao, W.-H., & Deer, B. (1996). Lead-Acid Batteries with Optimum Current Collection at Grid Lugs. United Kingdom.

Nakhaie, D., Benhangi, P. H., Alfantazi, A., & Davoodi, A. (2014). The effect of grid configurations on potential and current density distributions in positive plate of

lead-acid battery via numerical modeling. Electrochimica Acta, 115, 189–196. http://doi.org/10.1016/j.electacta.2013.10.152.

Newman, J., & Tiedeman, W. (1975). Porouse-Electrode Theory with Battery Applications. AIChE Journal, 21(1), 25–41.

Nguyen, T. V., White, R. E., & Gu, H. (1990). The Effects of Separator Design on the Discharge Performance of a Starved Lead-Acid Cell. Journal of The Electrochemical Society, 137(10), 2998–3004. http://doi.org/10.1149/1.2086148.

Pascoe, P. E., & Anbuky, A. H. (2002). The behaviour of the coup de fouet of valve-regulated lead-acid batteries. Journal of Power Sources, 111(2), 304–319. http://doi.org/10.1016/S0378-7753(02)00316-6.

Pascoe, P. E., & Anbuky, A. H. (2004). A VRLA battery simulation model. Energy Conversion and Management, 45(7–8), 1015–1041. http://doi.org/10.1016/j.enconman.2003.08.014.

Pavlov, D. (2011). Lead-Acid Batteries: Science and Technology. Oxford: Elsevier B.V.

R. Vasant Kumar, Sarakonsri, T. (2010). Introduction to Electrochemical Cells. Retrieved October 25, 2016, from https://application.wiley-vch.de/books/sample/3527324070_c01.pdf.

R M Dell, D A J Rand, R. (Bob) D. B. (2001). Understanding Batteries. Cambridge: The Royal Society of Chemistry.

Ruetschi, P. (1977). Reveiw on the Lead-Acid Battery Science and Technology. J. Power Sources, 2(1977178), 3–24.

Sunu, W. G., & Burrows, B. W. (1982). Mathematical Model for Design of Battery Electrodes I. Potential distribution. Journal of The Electrochemical Society, 129(4), 688–695. http://doi.org/10.1149/1.2123952.

Technical Marketing Staff of Gates Energy Products. (1998). Rechargeable Batteries Applications Handbook. Washington: Butterworth-Heinemann.

Ter-Gazarian, A. G. (2011). Energy Storage for Power Systems. London: The Institution of Engineering and Technology.

Tverberg, G. (2015). BP Data Suggests We Are Reaching Peak Energy Demand. Retrieved September 28, 2016, from https://ourfiniteworld.com/2015/06/23/bp-data-suggests-we-are-reaching-peak-energy-demand.

Vaaler, L. E., Brooman, E. W., & Fuggiti, H. A. (1982). Computerized design and evaluation of improved electrodes for lead-acid batteries. Journal of Applied Electrochemistry, 12(6), 721–734. http://doi.org/10.1007/BF00617493.